

## PHYSIOLOGY

# Cross-talk between TSC2 and the extracellular matrix controls pulmonary vascular proliferation and pulmonary hypertension

Yuanjun Shen<sup>1</sup>, Dmitry A. Goncharov<sup>1</sup>, Andressa Pena<sup>2</sup>, Jeffrey Baust<sup>2</sup>, Andres Chavez Barragan<sup>2</sup>, Arnab Ray<sup>2</sup>, Analise Rode<sup>2</sup>, Timothy N. Bachman<sup>2</sup>, Baojun Chang<sup>2</sup>, Lifeng Jiang<sup>1</sup>, Paul Dieffenbach<sup>3</sup>, Laura E. Fredenburgh<sup>3†</sup>, Mauricio Rojas<sup>4</sup>, Horace DeLisser<sup>5</sup>, Ana L. Mora<sup>4</sup>, Tatiana V. Kudryashova<sup>1</sup>, Elena A. Goncharova<sup>1\*</sup>

Copyright © 2022  
The Authors, some  
rights reserved;  
exclusive licensee  
American Association  
for the Advancement  
of Science. No claim  
to original U.S.  
Government Works

Increased proliferation and survival of cells in small pulmonary arteries (PAs) drive pulmonary arterial hypertension (PAH). Because cell growth mediated by the mTOR-containing mTORC1 complex is inhibited by tuberous sclerosis complex 2 (TSC2), we investigated the role of this GTPase-activating protein in PAH pathology. TSC2 abundance was decreased in remodeled small PAs and PA vascular smooth muscle cells (PAVSMCs) from patients with PAH or from rodent pulmonary hypertension (PH) models, as well as PAVSMCs maintained on substrates that reproduced pathology-induced stiffness. Accordingly, mice with smooth muscle–specific reduction in TSC2 developed PH. At the molecular level, decreased TSC2 abundance led to stiffness-induced PAVSMC proliferation, increased abundance of the mechanosensitive transcriptional coactivators YAP/TAZ, and enhanced mTOR kinase activity. Moreover, extracellular matrix (ECM) produced by TSC2-deficient PAVSMCs stimulated the proliferation of nondiseased PA adventitial fibroblasts and PAVSMCs through fibronectin and its receptor, the  $\alpha_5\beta_1$  integrin. Reconstituting TSC2 in PAVSMCs from patients with PAH through overexpression or treatment with the SIRT1 activator SRT2104 decreased YAP/TAZ abundance, mTOR activity, and ECM production, as well as inhibited proliferation and induced apoptosis. In two rodent models of PH, SRT2104 treatment restored TSC2 abundance, attenuated pulmonary vascular remodeling, and ameliorated PH. Thus, TSC2 in PAVSMCs integrates ECM composition and stiffness with pro-proliferative and survival signaling, and restoring TSC2 abundance could be an attractive therapeutic option to treat PH.

## INTRODUCTION

Pulmonary arterial hypertension (PAH) is a progressive and rapidly fatal disease with a high mortality rate and no cures (1) and is a serious public health problem with increasing death and hospitalization rates (2–4). In PAH, vasoconstriction and remodeling of small pulmonary arteries (PAs) (5–10) lead to chronically increased PA pressure (PAP), right ventricular (RV) afterload, and eventually, right ventricle failure and death (4). Available therapies fail to reverse established pulmonary vascular remodeling or prevent disease progression (5, 9), and development of novel antiproliferative/antiremodeling therapies is an unmet important need.

Increased proliferation and survival of resident pulmonary vascular cells, a key component of PA remodeling (8, 11, 12), are induced by the combination of soluble stimuli, such as excessive production of growth factors and proinflammatory mediators, and of physical factors, such as stiffening and remodeling of the extracellular matrix (ECM). As PAH progresses, PA vascular smooth muscle (VSM) cells (PAVSMCs) undergo a switch to the secretory,

proliferative, apoptosis-resistant phenotype, which is self-supported by constitutive inhibition of the growth suppressor HIPPO–large tumor suppressor 1 (LATS1) pathway and consequent up-regulation of its pro-proliferative downstream effectors, the transcriptional coactivators Yes-associated protein (YAP)/transcriptional coactivator with PDZ-binding motif (TAZ) and the mechanistic target of rapamycin (mTOR) complex 1 (mTORC1) and mTORC2 (7–9, 12–15). The mechanisms coordinating growth-promoting signals with proliferative responses of resident PA cells in PAH are not completely understood, and clinical use of available antiproliferative therapeutic strategies is challenging because of their side effects.

The growth suppressor tuberous sclerosis complex 2 (TSC2) (tuberin) inhibits mTORC1, cell growth, and proliferation (16). Deficiency or mutational inactivation of TSC2 is linked to proliferative diseases such as cancer, tuberous sclerosis, and pulmonary lymphangioleiomyomatosis (LAM) (16–18). Several lines of evidence suggest that TSC2 may act as a coordinator of mTORC1 and HIPPO-YAP/TAZ pathways in PAH pulmonary vasculature. First, mTORC1 is activated in remodeled small PAs and contributes to human PAH PAVSMC proliferation, VSM remodeling, and experimental pulmonary hypertension (PH) in mice (7, 19, 20). Second, mTOR-induced accumulation of YAP is reported in TSC2-null cells (21). In addition, PH develops in mice with VSM-specific knock-down of TSC1 (a binding partner of TSC2 that protects it from degradation) (22). Last, a subset of patients with pulmonary LAM (caused by somatic mutations or loss of heterozygosity in TSC) develop disproportionate precapillary PH that cannot be fully

<sup>1</sup>Lung Center, Division of Pulmonary, Critical Care and Sleep Medicine, University of California, Davis School of Medicine, Davis, CA 95616, USA. <sup>2</sup>Pittsburgh Heart, Lung, Blood and Vascular Medicine Institute, University of Pittsburgh School of Medicine, Pittsburgh, PA 15213, USA. <sup>3</sup>Division of Pulmonary and Critical Care Medicine, Brigham and Women's Hospital, Boston, MA 02115, USA. <sup>4</sup>Division of Pulmonary, Critical Care and Sleep Medicine, Ohio State University College of Medicine, Columbus, OH 43210, USA. <sup>5</sup>Department of Pathology and Laboratory Medicine, Pulmonary Vascular Disease Program, University of Pennsylvania Perelman School of Medicine, Philadelphia, PA 19104, USA.

\*Corresponding author. Email: eagoncharova@ucdavis.edu

†Present address: Regeneron Pharmaceuticals, Tarrytown, NY 10591, USA.

explained by hypoxemia and is likely attributable to the loss of pulmonary vascular TSC function (23).

In the present study, we sought to determine the role of TSC2 in pulmonary vascular hyperproliferation in PAH. We found that TSC2 acted as a mechanosensor and mechanotransducer, and its deficiency in smooth muscle cells from small PAs permitted up-regulation of YAP-TAZ and mTOR; increased PAVSMC proliferation, survival, and remodeling; and promoted PH. We also mechanistically linked PAVSMC-specific TSC2 deficiency to excessive ECM production, ECM-dependent activation of YAP/TAZ and mTOR, and increased growth of PAVSMCs and PA adventitial fibroblasts (PAAFs). Last, we demonstrated that TSC2 restoration by SRT2104 was beneficial in inhibiting YAP/TAZ and mTOR, reversing pulmonary vascular remodeling, and reducing PH.

## RESULTS

### TSC2 abundance is decreased in PAVSMCs from human PAH lungs

To determine the status of TSC2 in human PAH lungs, we performed immunohistochemical and immunoblot analysis of lung tissue specimens from individuals with PAH and from nondiseased (control) donors (table S1). We found that TSC2 protein levels were lower in smooth muscle  $\alpha$ -actin (SMA)-positive areas and whole-tissue lysates of small PAs from PAH lungs compared with those from control lungs (Fig. 1, A to D). Supporting our observations, PAVSMCs from small (<1.5-mm outer diameter) human PAH PAs had significantly reduced TSC2 protein content (Fig. 1, E and F) and significantly higher nonstimulated proliferation than those from nondiseased individuals (Fig. 1, G and H). TSC2 abundance was not changed in human PAH PA endothelial cells (PAECs) or PAAFs (fig. S1, A to D). Together, these data demonstrate that TSC2 is deficient in PAVSMCs in remodeled small PAs in human PAH lungs.

### Reduced TSC2 abundance enables PAVSMC hyperproliferation, remodeling, and PH

To determine the functional outcome of decreased TSC2 content, we depleted TSC2 in human control PAVSMCs by small interfering RNA (siRNA), which significantly increased DNA synthesis [as assessed by bromodeoxyuridine (BrdU) incorporation] and cell proliferation (Fig. 1, I to K). To test the in vivo consequences of TSC2 deficiency, we generated mice with SMC-specific *Tsc2* knockout by crossing *Tsc2*<sup>fllox/flox</sup> mice and *Tagln* (*Sm22*)-*cre* mice (13). Homozygous knockout of *Tsc2* was embryonically lethal. Mice with heterozygous deletion of *Tsc2* (*Tsc2*<sup>+/-</sup>) (fig. S2, A and B) developed spontaneous mild experimental PH as early as 9 weeks of age. Compared with the same-age wild-type (WT) controls, 9-week-old male *SM22-Tsc2*<sup>+/-</sup> mice had significantly greater medial thickness of small (<150  $\mu$ m) PAs (PA MT) (Fig. 1, L and M), elevated systolic RV pressure (sRVP) (Fig. 1N), and RV hypertrophy [as determined by the significant increase in the RV/(LV + S) ratio] (Fig. 1O). Four of six female mice also developed mild experimental PH (sRVP  $\geq$  30 mmHg) at 9 weeks of age (fig. S3A). Exposing 9-week-old *SM22-Tsc2*<sup>+/-</sup> mice to hypoxia (10% O<sub>2</sub>, 3 weeks) resulted in significantly higher PA MT for male mice and RV hypertrophy for both male and female mice (fig. S3, B to G) without altering sRVP compared with same-sex same-age controls (fig. S3, H and I). Twenty-two-week-old male *SM22-Tsc2*<sup>+/-</sup> mice, but not their female

counterparts, had significant pulmonary vascular remodeling compared with same-age controls and significantly greater RV hypertrophy than 9-week-old *SM22-Tsc2*<sup>+/-</sup> mice (fig. S4, A to G), suggesting that the experimental PH phenotype continued to develop. Together, these data demonstrate that reduced TSC2 abundance results in increased PAVSMC proliferation, VSM remodeling, and spontaneous experimental PH.

### Decreased TSC2 content is induced by substrate stiffening and enables YAP/TAZ accumulation and PAVSMC proliferation

To identify pro-PAH stimuli that induce TSC2 deficiency in PAVSMCs, we exposed control human PAVSMCs to various soluble growth factors and proinflammatory mediators (platelet-derived growth factor-BB (PDGF-BB), insulin growth factor 1, interleukin-6, tumor necrosis factor- $\alpha$ , and endothelin-1). We also maintained the cells on matrices of different compositions (collagen 1, collagen IV, fibronectin, and laminin) or stiffnesses (0.2 kPa, a stiffness seen under normal physiological conditions, and 25 kPa, a stiffness seen under pathological conditions) (8, 11, 13). We found that TSC2 protein levels showed a trend to decrease in PAVSMCs maintained on the collagen 1 matrices or treated with PDGF-BB (Fig. 2, A to D) and that PDGF-dependent increases in the phosphorylation Akt and, in part, ribosomal protein S6 were attenuated in control PAVSMCs treated with the PDGF receptor inhibitor AG1295 (fig. S5, A to C). These data agree with previously published studies demonstrating that PDGF inhibits TSC2-mTORC1 signaling through Akt (24).

Maintenance of PAVSMCs on stiff (25 kPa) (8, 12, 14, 15) matrices reduced TSC2 protein content and significantly increased cell proliferation compared with the cells seeded on soft (0.2 kPa) substrates (Fig. 2, E to G). To determine whether TSC2 modulates stiffness-induced PAVSMC proliferation, we transfected control human PAVSMCs seeded on stiff (25 kPa) matrices with mammalian vectors expressing green fluorescent protein (GFP)-TSC2 or control GFP. GFP-TSC2-transfected PAVSMCs had about twofold lower proliferation on stiff matrices than GFP-transfected cells (Fig. 2H), suggesting that TSC2 acts as a mechanosensor and mechanotransducer and that decreased TSC2 abundance in PAVSMCs is induced by increased matrix stiffness and is required for stiffness-induced cell proliferation.

Stiffening of small PAs drives pulmonary vascular cell proliferation and remodeling in PAH through the transcriptional coactivators YAP/TAZ, which act partially by promoting pro-proliferative and survival signaling through the Akt-mTOR pathway (8, 12, 14). Reexpression of TSC2 in control PAVSMCs maintained on stiff matrices not only significantly decreased the phosphorylation of the ribosomal protein S6, a hallmark of mTORC1 activation, but also significantly reduced YAP/TAZ protein levels compared with those in GFP-expressing cells (Fig. 2, I and J). Supporting our findings, siRNA-mediated depletion of TSC2 in control human PAVSMCs resulted in a significant increase in S6 and Akt phosphorylation and accumulation of YAP/TAZ compared with cells transfected with control siRNA (Fig. 2, K and L). These data show that decreased TSC2 content in PAVSMCs is required for stiffness-induced PAVSMC proliferation and increases in YAP/TAZ abundance and mTOR activity.

PAVSMCs in PAH have an overaccumulation of active YAP in nuclei, leading to hyperproliferation and pulmonary vascular

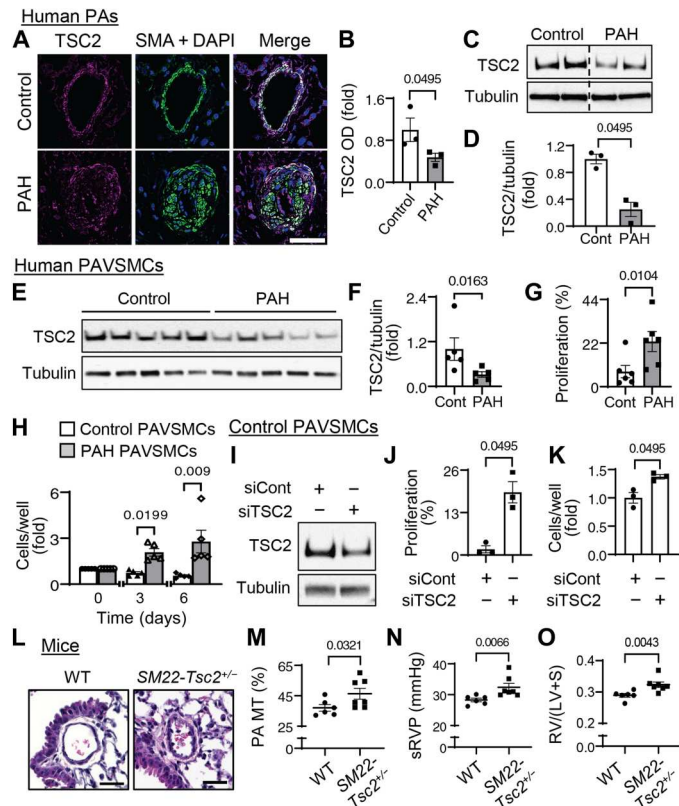


**Fig. 1. TSC2 deficiency results in increased PAVSMC proliferation, vascular remodeling, and PH.** (A) Immunohistochemical analysis of human lung tissue sections to detect TSC2 (magenta), SMA (green), and DAPI (blue). Scale bar, 100  $\mu$ m. Images are representative of three individuals per group, six PAs per individual. (B) Optical density (OD) measurement of TSC2 fluorescent signal in SMA-positive regions of human small PAs. Data are means  $\pm$  SE from three individuals per group, six PAs per individual, 12 areas per PA. PAH was normalized to control, which was set at 1. *P* value for PAH compared to control was determined by Mann-Whitney *U* test. Images from different parts of the same gel are separated by a dashed line. (C and D) Immunoblot analysis of small PAs. Data are means  $\pm$  SE from *n* = 3 individuals per group. *P* values for PAH compared to control was determined by Mann-Whitney *U* test. (E and F) Immunoblot analysis of human nondiseased (control) (white bars) and PAH (gray bars) PAVSMCs. Data are means  $\pm$  SE. PAH was normalized to control which was set to 1. *n* = 5 individuals per group. *P* values for PAH compared to control was determined by Mann-Whitney *U* test. (G) Proliferation of human control and PAH PAVSMCs as measured by Ki67 staining. Data represent percentage of Ki67-positive cells per total number of cells (as detected by DAPI) and are means  $\pm$  SE from *n* = 6 individuals per group. *P* values for PAH compared to control was determined by Mann-Whitney *U* test. (H) Equal quantity of cells was plated on each well of six-well plate (day 0), and cell counts were performed at days 3 and 6. Data are fold change to day 0. Data are means  $\pm$  SE from *n* = 5 individuals per group. *P* values for PAH compared to control were determined by Mann-Whitney *U* test. (I to K) Immunoblot (I), proliferation as measured by BrdU incorporation (J) or cell counting (K) performed on control human PAVSMCs transfected with siRNA directed against TSC2 (siTSC2) or control siRNA GLO (siCont) for 48 hours. Data are means  $\pm$  SE from *n* = 3 individuals per group. *P* values for siTSC2 compared to siCont were determined by Mann-Whitney *U* test. (L to O) Morphological and hemodynamic analysis of 9-week-old male *SM22-Tsc2*<sup>+/-</sup> and wild-type (WT) mice. Images (L) are representative of six mice per group, 12 PAs per mouse. Scale bars, 30  $\mu$ m. Graphs show PA medial thickness (PA MT) (M), systolic RV pressure (sRVP) (N), and Fulton index [right ventricle (RV)/(left ventricle (LV) + septum)] (O). Data are means  $\pm$  SE for *n* = 6 WT mice and *n* = 7 *SM22-Tsc2*<sup>+/-</sup> mice. *P* values for *SM22-Tsc2*<sup>+/-</sup> compared to WT by Mann-Whitney *U* test.

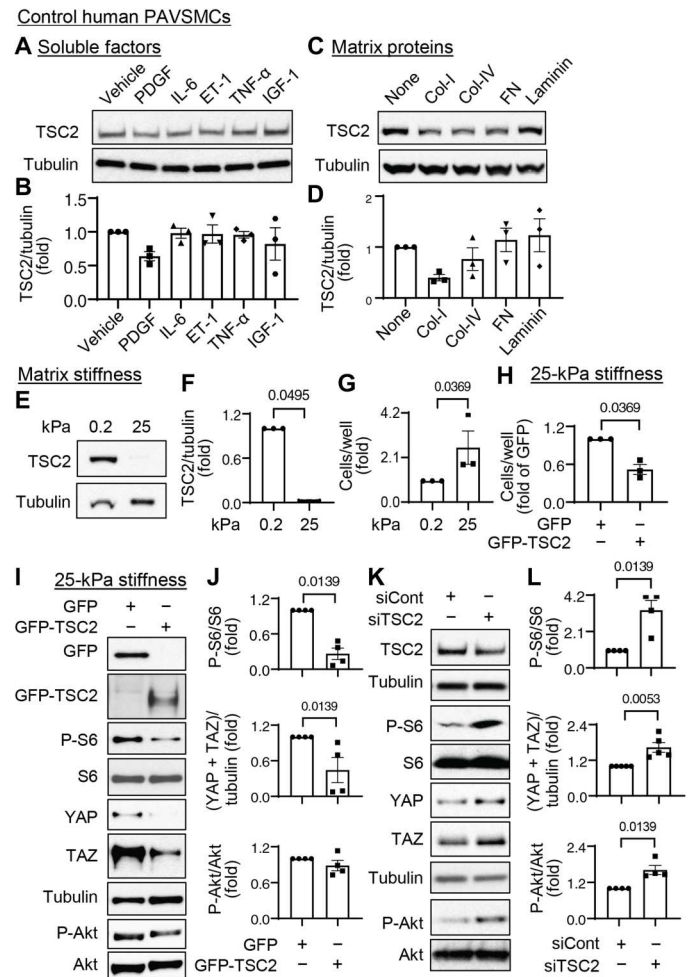


**Fig. 2. Decreased TSC2 content is induced by increased substrate stiffness and is required for YAP/TAZ accumulation, activation of Akt and mTOR, and increased PAVSMC proliferation.** (A to D) Immunoblot analysis of control human PAVSMCs treated with the indicated soluble factors (A and B) or maintained on the indicated matrices (C and D) for 48 hours. Data are means  $\pm$  SE from *n* = 3 individuals per group. Values were normalized to vehicle treatment or uncoated matrix, which were set at 1. *P* values were determined by Kruskal-Wallis test with Dunn's pairwise comparison. (E and F) Immunoblot analysis of control human PAVSMCs maintained on softwell hydrogels with normal (0.2 kPa) or pathological (25 kPa) stiffness for 48 hours. Data are means  $\pm$  SE from *n* = 3 individuals per group. Twenty-five kilopascals was normalized to 0.2 kPa, which was set at 1. *P* values for 25 kPa compared to 0.2 kPa were determined by Mann-Whitney *U* test. (G) Equal numbers of control human PAVSMCs were plated on hydrogels with 0.2- or 25-kPa stiffness, and cell proliferation analysis was performed on day 4. Data are means  $\pm$  SE from *n* = 3 individuals per group. Twenty-five kilopascals was normalized to 0.2 kPa, which was set at 1. *P* values for 25 kPa compared to 0.2 kPa were determined by Mann-Whitney *U* test. (H to J) Human control PAVSMCs were plated on softwell hydrogels with 25-kPa stiffness and transfected with mammalian vectors expressing GFP or GFP-tagged human TSC2 for 36 hours. Cell proliferation (H) and immunoblot analyses (I and J) were performed. Data are means  $\pm$  SE from *n* = 3 (cell counts) and 4 (immunoblots) individuals per group. GFP-TSC2 was normalized to GFP, which was set at 1. *P* values for GFP-TSC2 compared to GFP were determined by Mann-Whitney *U* test. (K and L) Human control PAVSMCs were transfected with siRNA directed against TSC2 (siTSC2) or control siRNA GLO (siCont) for 48 hours and were immunoblotted for the indicated proteins. Data are means  $\pm$  SE from *n* = 4 or 5 individuals per group. siTSC2 was normalized to siCont, which was set at 1. *P* values for siTSC2 compared to siCont were determined by Mann-Whitney *U* test.



remodeling (8, 11, 12, 14). YAP could be phosphorylated at Ser<sup>127</sup> by LATS1/2 and Akt, leading to its cytoplasmic retention and inhibition (25, 26). We observed no differences in the phosphorylation of Ser<sup>127</sup> in YAP in human PAH PAVSMCs compared to controls (fig. S6, A and B) and in SMA-positive areas of small PAs from *SM22-Tsc2*<sup>+/-</sup> mice compared to WT animals (fig. S6, C and D). Treatment of human PAH PAVSMCs with the LATS1/2 kinase inhibitor LATS-IN-1 (27) significantly reduced the phosphorylation of Ser<sup>127</sup> in YAP, an effect not observed with transfection of

siRNA Akt1/2, which also did not affect LATS-IN-1–dependent inhibition of this phosphorylation event (fig. S7, A and B). Together with published studies, these data suggest that LATS, rather than Akt, is responsible for the phosphorylation of Ser<sup>127</sup> in YAP in human PAH PAVSMCs.

Akt1 is a key Akt isoform involved in pulmonary vascular remodeling (28), but cotransfection of siRNAs targeting TSC2 and Akt1 did not significantly reduce TSC2-dependent phosphorylation of S6K1 and S6 (fig. S8, A and B), suggesting that TSC2 loss

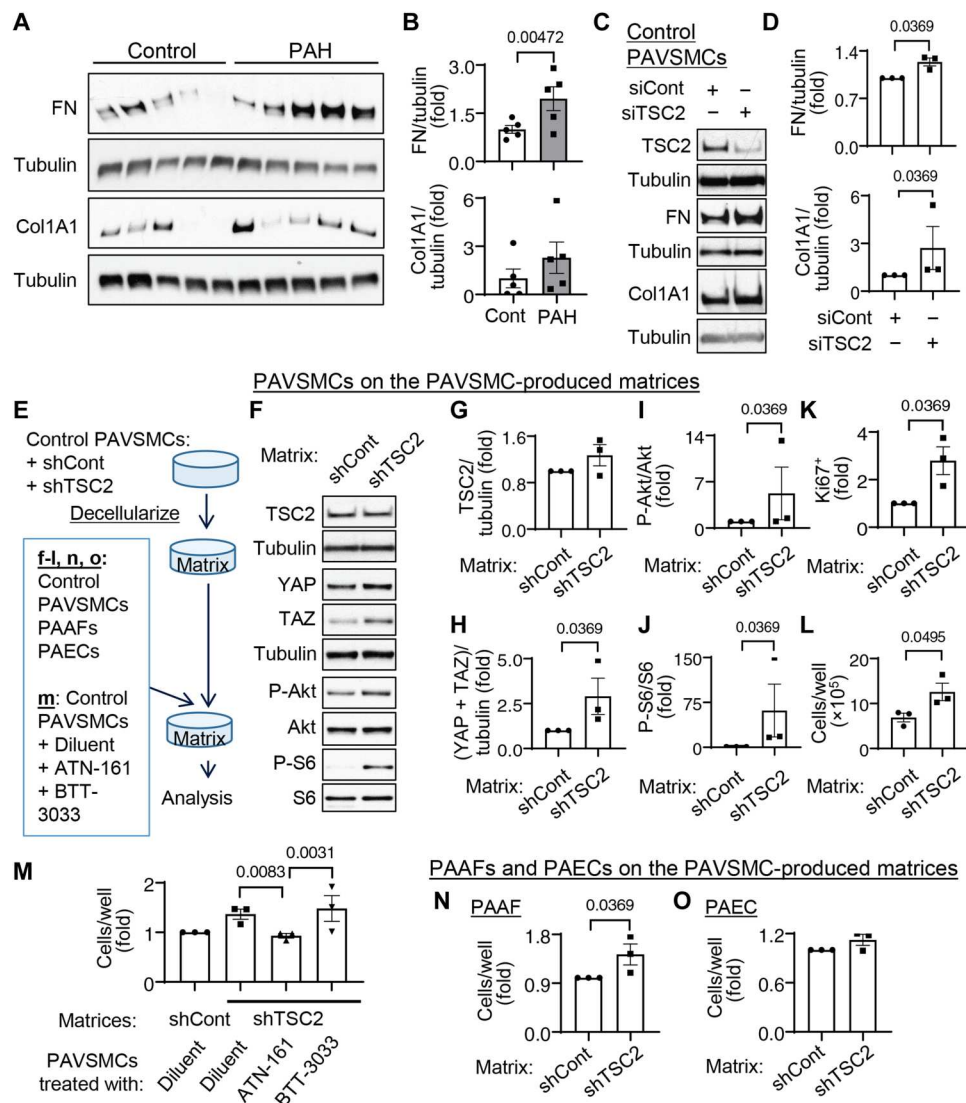


**Fig. 3. Reduced TSC2 abundance in PAVSMCs promotes YAP/TAZ accumulation, mTOR activity, and proliferation of nondiseased pulmonary vascular cells through ECM remodeling.** (A and B) Human control and PAH PAVSMCs (from five individuals per group) were immunoblotted for fibronectin (FN) and collagen 1A1 (Col1A1). Data are means  $\pm$  SE. PAH was normalized to Cont, which was set at 1.  $P$  values for PAH compared to Cont were determined by Mann-Whitney  $U$  test. (C and D) Human control PAVSMCs were transfected with siRNA directed against TSC2 (siTSC2) or control siRNA GLO (siCont) and immunoblotted for FN and Col1A1. Data are means  $\pm$  SE from  $n = 3$  individuals per group. siTSC2 was normalized to siCont, which was set at 1.  $P$  values for siTSC2 compared to siCont were determined by Mann-Whitney  $U$  test. (E to O) Preconfluent control PAVSMCs were infected with adenoviruses encoding control shRNA (shCont) or shRNA directed against TSC2 (shTSC2) for 6 days (E). Cells were removed and an equal amount of nondiseased (control) untreated PAVSMCs (F to L), PAVSMCs treated with diluent, 10  $\mu$ M ATN161 ( $\alpha_2\beta_1$  integrin inhibitor), or 10  $\mu$ M BTT3033 ( $\alpha_2\beta_1$  integrin inhibitor) (M), control PAAFs (N), or control PAECs (O) were plated on the matrices. Four days after plating, immunoblot (F to J) and proliferation analyses as measured by Ki67 staining (K) or cell counting (L to O) were performed. Data are means  $\pm$  SE from  $n = 3$  individuals per group.  $P$  values for siTSC2 compared to siCont were determined by Mann-Whitney  $U$  test (significance) (G to L, N, and O) and by Kruskal-Wallis test with Dunn's pairwise comparison (M).

attenuates Akt-dependent mTORC1 activation. To confirm our observations, we used rat Eker leiomyoma tumor 3 (ELT3) cells, which carry a germline *Tsc2* mutation, resulting in TSC2 loss and constitutive mTORC1 activation (fig. S8C) (29). Treatment of ELT3 cells with the Akt inhibitor VIII did not affect S6K1 and S6 phosphorylation (fig. S8, D and E), demonstrating that TSC2 deficiency compromises Akt-dependent mTORC1 activation.

### Decreased TSC2 content promotes increases in YAP/TAZ abundance, mTOR activity, and PAVSMC proliferation through ECM remodeling

Because YAP and TAZ facilitate resident pulmonary vascular cell proliferation in PAH through ECM remodeling (8, 11), we hypothesized that, in addition to canonical Rheb-dependent activation of mTORC1, reduced TSC2 abundance in PAH PAVSMCs may facilitate pro-proliferative signaling by modulating ECM production. In agreement with previous studies (8, 11), PAVSMCs from human PAH lungs had higher fibronectin and collagen 1A protein content compared with those from control lungs (Fig. 3, A and B). Moreover, TSC2 knockdown significantly increased fibronectin and collagen 1A protein levels in control human PAVSMCs (Fig. 3, C and D), suggesting that decreased TSC2 content facilitates production of the two key ECM proteins involved in PAH. Because excessive ECM production promotes stiffening of small muscular PAs (30), we next tested the effect of smooth muscle TSC2 loss on pulmonary vascular wall stiffness using atomic force microscopy (AFM) analysis. Mechanical characterization of small (<200  $\mu$ m in diameter) PAs by AFM microindentation (15) revealed that 9-week-old male *SM22-Tsc2<sup>+/-</sup>* mice had significantly higher vascular wall stiffness compared with WT mice (fig. S9, A and B). Together, these data demonstrate that a decrease in smooth muscle TSC2 elevates ECM production and induces pulmonary vascular wall stiffening.

Next, we evaluated whether reduced TSC2 abundance modulated pro-proliferative signaling in neighboring cells through the ECM. We used decellularized matrices from control human PAVSMCs infected with lentiviruses producing TSC2 short hairpin RNA (shRNA) (shTSC2) or control shRNA as substrates for the plating of control human PAVSMCs (Fig. 3E). We found that control PAVSMCs seeded on matrices produced by shTSC2-infected control PAVSMCs had significantly higher YAP/TAZ protein levels, increased phosphorylation of Ser<sup>473</sup> in Akt and of S6, and elevated proliferation compared with cells seeded on matrices produced by shCont-infected PAVSMCs (Fig. 3, F to L). To further confirm the role of ECM in the increase in YAP/TAZ abundance, Akt phosphorylation, mTOR activity, and cell proliferation in TSC2-deficient PAVSMCs, we maintained control PAVSMCs on cell-free matrices produced by shTSC2-infected PAVSMCs in the presence of ATN-161, a small peptide antagonist of  $\alpha_5\beta_1$  integrin, and BTT-3033, a selective inhibitor of  $\alpha_2\beta_1$  integrin, to block cell binding with fibronectin and collagen, respectively (Fig. 3E). ATN-161, but not BTT3033, prevented matrix-induced PAVSMC proliferation (Fig. 3M), suggesting that decreased TSC2 abundance promotes PAVSMC proliferation by regulating extracellular fibronectin content. Supporting the relevance of these findings to human PAH, control PAVSMCs seeded at the decellularized ECM produced by human PAH PAVSMCs showed increases in the phosphorylation of Ser<sup>473</sup> in Akt and of S6 and in YAP/TAZ protein content compared with cells maintained on matrices produced by

nondiseased PAVSMCs (fig. S10, A to F). Collectively, these data demonstrate that TSC2 deficiency promotes increases in YAP/TAZ abundance, mTOR activity, and PAVSMC proliferation through ECM remodeling.

In contrast to stiffness-induced TSC2 deficiency (Fig. 2, E and F), control PAVSMCs seeded on the matrices produced by TSC2-deficient control or PAH PAVSMCs showed increased YAP/TAZ abundance and mTOR activity without a reduction in TSC2 protein levels (Fig. 3, F to I, and fig. S10, A to F). These data support our observations that TSC2 acts upstream of YAP/TAZ and mTOR by regulating the ECM and suggest an ECM composition-independent mechanism(s) that maintains a self-sustaining suppression of TSC2 content in PAH PAVSMCs. We observed no significant differences in the protein levels of TSC2 binding partner TSC1 (17, 31) in SMA-positive areas of small PAs from *SM22-Tsc2<sup>+/-</sup>* and control mice and in human PAVSMCs from control and PAH individuals (fig. S11, A to D). Because mTOR acts both upstream (through mTORC2) and downstream (through mTORC1) of TSC2 (17), and because the activity of both mTORC2 and mTORC1 is increased by YAP/TAZ in human PAH PAVSMCs (7, 8), we hypothesized that stiffness-independent TSC2 deficiency could be self-supported by a YAP/mTORC2 feed-forward loop. Supporting our hypothesis, siRNA-mediated depletion of YAP and disruption of mTORC2 by siRNA-mediated depletion of Rictor led to TSC2 accumulation in human PAH PAVSMCs compared with cells transfected with control siRNA (figs. S12, A and B, and S13, A to C). Moreover, cotransfection with TSC2 siRNA reversed the Rictor siRNA-induced decrease in PAH PAVSMC proliferation (fig. S13, D and E), suggesting that mTORC2-dependent reduction of TSC2 protein levels is required for PAH PAVSMC proliferation. However, treatment of human PAH PAVSMCs with either the mTOR kinase inhibitor PP242 (which inhibits mTOR in both mTORC1 and mTORC2) or the allosteric mTORC1 inhibitor rapamycin did not increase TSC2 protein levels or reduce YAP/TAZ accumulation (fig. S14, A and B), suggesting that suppression of TSC2 abundance in PAH PAVSMCs is supported by YAP/mTORC2 independently of mTOR kinase activity.

### ECM produced by TSC2-deficient PAVSMCs induces PAAF proliferation

Because changes in ECM composition affect the proliferative response of neighboring pulmonary vascular cells, we next tested whether the matrix produced by TSC2-deficient PAVSMCs modulates the proliferation of other resident pulmonary vascular cells. We seeded control human PAECs and PAAFs on matrices produced by control human PAVSMCs infected with adenovirus producing shTSC2 or control shRNA (Fig. 3E). We found that control PAAFs, but not PAECs, had significantly higher cellular proliferation when maintained on matrices produced by shTSC2-infected PAVSMCs compared with cells seeded on the matrices produced by shCont-infected PAVSMCs (Fig. 3, N and O). These data show that TSC2 deficiency in PAVSMCs results in dysregulated ECM production, which promotes PAAF proliferation.

### Restoration of TSC2 abundance suppresses proliferation and induces apoptosis in PAH PAVSMCs

We next sought to evaluate the potential benefits of restoring functional TSC2 in PAVSMCs from human PAH lungs. We found that

TSC2 expression suppressed Akt and S6 phosphorylation, YAP/TAZ protein levels, and fibronectin and collagen 1A production compared with GFP-expressing cells (Fig. 4, A and B, and fig. S15a). Moreover, expression of TSC2 suppressed PAH PAVSMC proliferation (Fig. 4C and fig. S15B) and induced the accumulation of cleaved caspase-3 and significant apoptosis (Fig. 4, D and E), suggesting that restoration of TSC2 may be a possible therapeutic strategy to suppress both YAP/TAZ and mTOR pathways, halt excessive ECM production, inhibit proliferation, and induce apoptosis in PAH PAVSMCs.

### **SRT2104 reverses the PAVSMC phenotype in PAH by restoring TSC2 abundance**

Next, we evaluated potential pharmacological strategies to restore functional TSC2 in human PAH PAVSMCs. TSC2 is regulated by direct phosphorylation, which either prevents or promotes its degradation (17), and other types of posttranslational modification, such as deacetylation by sirtuin 1 (SIRT1) (32). Positive and negative regulators of TSC2 involved in PAH are Akt and adenosine monophosphate-activated protein kinase (AMPK). Akt is activated, whereas AMPK is inhibited, in human PAH PAVSMCs, and either inhibition of Akt or activation of AMPK suppresses mTORC1 and PAH PAVSMC proliferation (8, 19, 28, 33–36). We found that pharmacological inhibition of Akt or activation of AMPK reduced S6 phosphorylation but did not elevate TSC2 protein content (fig. S16, A and B). Together with the inability of mTORC1/2 inhibitor PP242 to restore TSC2 abundance in PAH PAVSMCs, our data suggest that mTOR, Akt, and AMPK act downstream of or in parallel to TSC2 and that targeting these signaling proteins cannot restore PAH-specific TSC2 deficiency.

Next, we tested the effect of the SIRT1 activator SRT2104. We found that treatment of human PAH PAVSMCs with SRT2104 significantly increased TSC2 protein levels and suppressed S6 phosphorylation (Fig. 5, A to C), showing that SRT2104 restores functional TSC2. Moreover, SRT2104 significantly decreased the phosphorylation of Ser<sup>473</sup> in Akt and the abundance of collagen 1A and fibronectin, showed a trend in reducing YAP/TAZ accumulation (Fig. 5, A and D to H), and significantly inhibited proliferation and promoted apoptosis in PAH PAVSMCs (Fig. 5, I to K). In addition, SRT2104 also reduced the proliferation of control PAVSMCs on stiff matrices (Fig. 5L), suggesting potential benefits of SRT2104 in targeting both self-sustaining and stiffness-induced PAVSMC proliferation in PAH. To test whether SRT2104 acted through TSC2, we targeted TSC2 by siRNA in SRT2104-treated cells. We found that siRNA-mediated knockdown of TSC2 prevented SRT2104-induced inhibition of S6 phosphorylation and of cell proliferation and blocked SRT2104-induced apoptosis (Fig. 5, M to Q). Together, the data show that restoration of TSC2 abundance by SRT2104 inhibits proliferation and induces apoptosis in human PAH PAVSMCs.

### **SRT2104 restores TSC2 in small PAs and reduces established PH in mice and rats**

We examined whether short-term treatment of mice with SRT2104 after the establishment of SU5416/hypoxia (SuHx)-induced experimental PH led to TSC2 accumulation in small PAs (Fig. 6A). Similar to human PAH PAVSMCs, vehicle-treated mice from the SuHx group had reduced TSC2 protein levels in SMA-positive areas of small PAs (Fig. 6B), suggesting similar underlying

mechanisms. As expected, these mice developed pulmonary vascular remodeling and experimental PH as evidenced by significantly higher PA medial thickness (PA MT), sRVP, PAP, and RV hypertrophy (Fig. 6, B to F). The SRT2104-treated mice had higher TSC2 protein content in small PAs and significantly lower PA MT, sRVP, PAP, and RV hypertrophy compared with vehicle-treated SuHx mice (Fig. 6, B to F). There were no significant differences between male and female mice. Systolic left ventricular (LV) pressure (sLVP), mean arterial pressure (MAP), and heart rate did not significantly differ between vehicle- and SRT2104-treated groups (fig. S17, A to C). These data show that short-term SRT2104 treatment increases TSC2 abundance, attenuates VSM remodeling and PH, and improves RV hypertrophy in mice with SuHx-induced PH.

To evaluate the potential benefits of SRT2104 in severe experimental PH, we next tested the effects of long-term SRT2104 treatment using a rat SuHx model of experimental PH (Fig. 7A). Similar to human PAH PAVSMCs and the mouse PH model (Figs. 1A and 6B), vehicle-treated rats with SuHx-induced PH developed VSM-specific TSC2 deficiency in remodeled small PAs and robust pulmonary vascular remodeling, which were reversed by treatment with SRT2104 (Fig. 7, B to D). SuHx-exposed rats developed experimental PH and RV hypertrophy compared with control rats (Fig. 7, E to H). Treatment with SRT2104, but not vehicle, normalized sRVP and PAP and improved RV morphology and function (as shown by reversals of RV hypertrophy and normalized max dP/dT and the contractility index) (Fig. 7, E to I). There were no significant differences in sLVP, MAP, and heart rate between SuHx + vehicle and SuHx + SRT2104 groups (fig. S17, D to F). Together, these data demonstrate that SRT2104 reverses established PH and improves RV morphology and function in a severe irreversible rat model of experimental PH.

## **DISCUSSION**

The present study provides evidence that reduced TSC2 abundance in the medial layer of small PAs is an important trigger of PH and suggests that the restoration of functional TSC2 may be an attractive therapeutic strategy to reverse existing pulmonary vascular remodeling and PH. We found that TSC2 content was decreased in remodeled small PAs from individuals with PAH, two models of experimental PH, and early-passage PAVSMCs derived from small PAs of patients with PAH. Reduced abundance or loss of TSC2 decreased PAVSMC hyperproliferation, survival, pulmonary vascular remodeling, and development of spontaneous PH. Moreover, TSC2 in PAVSMCs acted as a mechanosensor and mechanotransducer and prevented the increases in YAP/TAZ abundance, mTOR activity, and cell proliferation induced by pathological stiffness. In addition, TSC2 controlled ECM composition, and reduced abundance or loss of TSC2 enhanced the production of abnormal ECM that resulted in increases in YAP/TAZ abundance, mTOR activity, and proliferation of PAVSMCs and PAAFs. Last, pharmacological restoration of functional TSC2 by SRT2104 reversed molecular abnormalities, inhibited proliferation, induced apoptosis in human PAH PAVSMCs, and reduced established pulmonary vascular remodeling and PH in two rodent models of experimental PH (Fig. 8).

Increased proliferation and resistance to apoptosis of pulmonary vascular cells in small PAs underlie pulmonary vascular remodeling, a key component of PAH pathogenesis. Here, we showed that



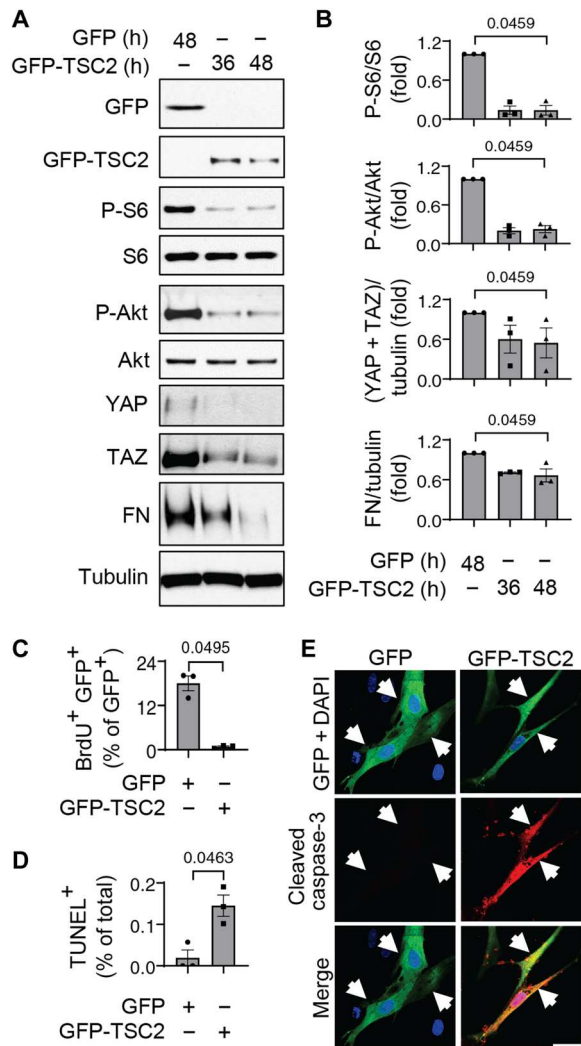


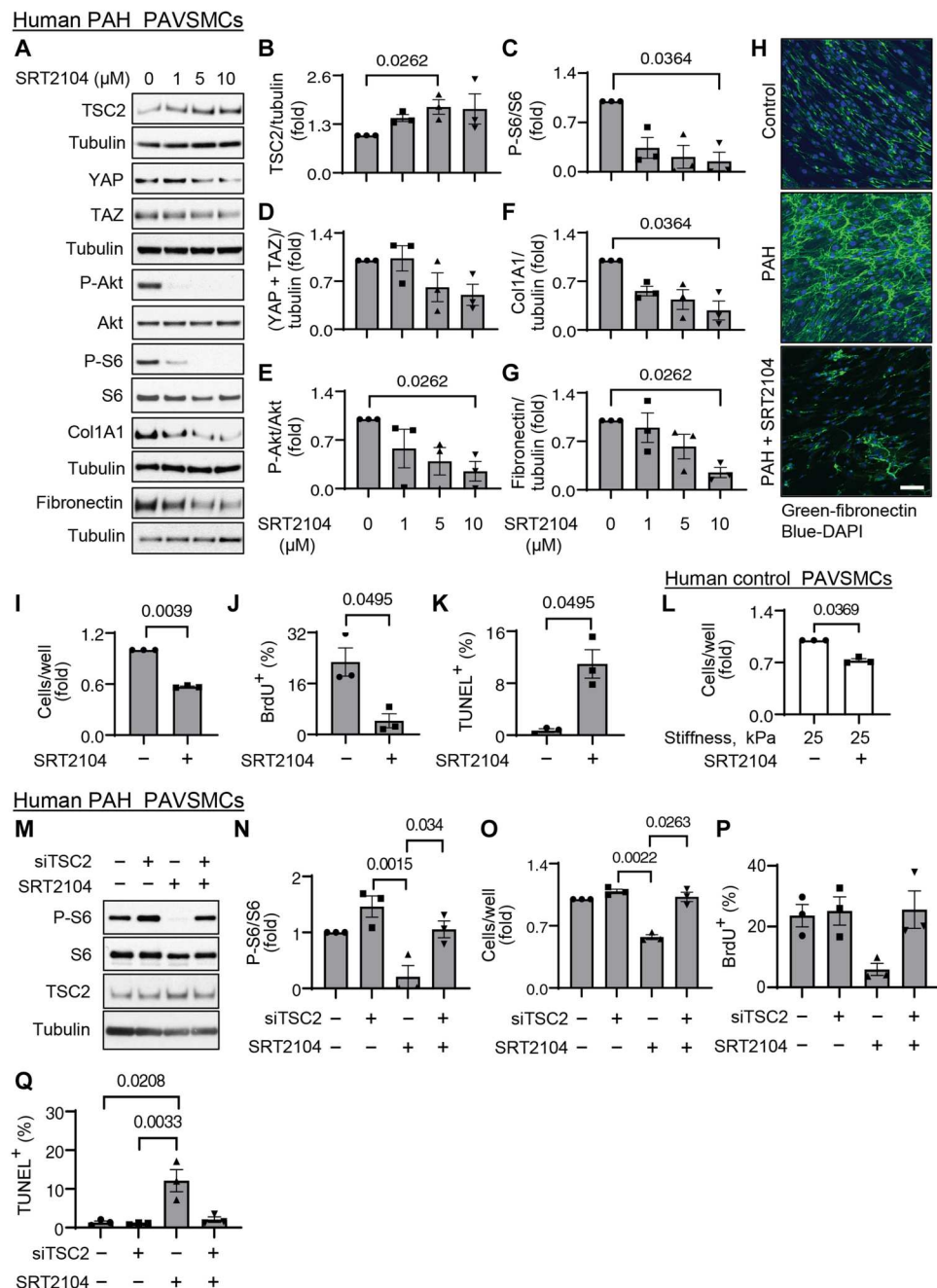
**Fig. 4. TSC2 reconstitution reduces YAP/TAZ accumulation and fibronectin production, suppresses proliferation, and induces apoptosis in human PAH PAVSMCs.** (A and B) Human PAH PAVSMCs were transfected with GFP or GFP-TSC2 for the indicated times and immunoblotted to detect the indicated proteins. Data are means  $\pm$  SE from three individuals per group. *P* values for GFP-TSC2 compared to GFP were determined by Kruskal-Wallis rank test with Dunn's pairwise comparison. (C to E) Proliferation (as measured BrdU incorporation) (C), apoptosis (as measured by TUNEL staining) (D), and immunocytochemical analysis to detect cleaved caspase-3 (red), GFP (green), and DAPI (blue) (E). Data are means  $\pm$  SE from three individuals per group. A minimum of 12 transfected cells per individual and condition were analyzed. *P* values for GFP-TSC2 compared to GFP were determined by Mann-Whitney *U* test. Scale bar, 50  $\mu$ m. White arrows indicate transfected cells.

TSC2, a key inhibitor of mTORC1 and cell proliferation (37), was decreased in abundance in proliferative PAVSMCs, small remodeled PAs from human PAH lungs, and two rodent models of experimental PH. Our data indicated that reduced TSC2 content in PAVSMCs resulted in the unstimulated growth and proliferation of nondiseased human PAVSMCs, and SMC-specific *Tsc2* heterozygosity in mice led to pulmonary vascular remodeling and early onset of spontaneous PH, indicating that even partial depletion of smooth muscle *Tsc2* was sufficient to induce pulmonary vascular remodeling and PH.

A switch to the hyperproliferative, apoptosis-resistant PAVSMC phenotype could be induced by various pro-PH factors, including exposure to soluble mitogens and changes in the ECM composition and stiffness (9, 38, 39). We found that decreased TSC2 content induced by pathological matrix stiffening was required for stiffness-induced proliferation of PAVSMCs, suggesting that TSC2 acts as a mechanosensor and a mechanotransducer. In addition to pathological stiffness, TSC2 abundance was reduced, although to a lesser extent, by its upstream inhibitor PDGF (37), suggesting the multifactorial nature of TSC2 regulation. We found that TSC2 loss was required for the accumulation of the pro-proliferative/pro-survival mechanotransducers YAP/TAZ, which are implicated in the pathogenesis of PAH (8, 12, 40) and increased activity of the Akt-mTOR axis, suggesting that TSC2 integrates the mTOR and HIPPO networks, two major regulators of pulmonary vascular cell proliferation and survival in PAH (7–9, 41). Further, TSC2 regulates cellular metabolism, protein translation, and autophagy, and the loss or mutational inactivation of TSC2 in pulmonary LAM activates mTORC1, RhoA, and cyclin-dependent kinase 2 (42), pro-proliferative and vasoconstrictive molecules involved in PAH pathogenesis (43, 44). Although further studies are needed, TSC2 in PAH may integrate mechanobiological cues with PAVSMC contractility, cellular metabolism, proliferative signaling, and cell cycle progression. If so, the reduced TSC2 abundance that we observed in PAVSMCs from patients or disease models may be responsible for both vasoconstriction and pulmonary vascular remodeling, two major pathological features of PAH.

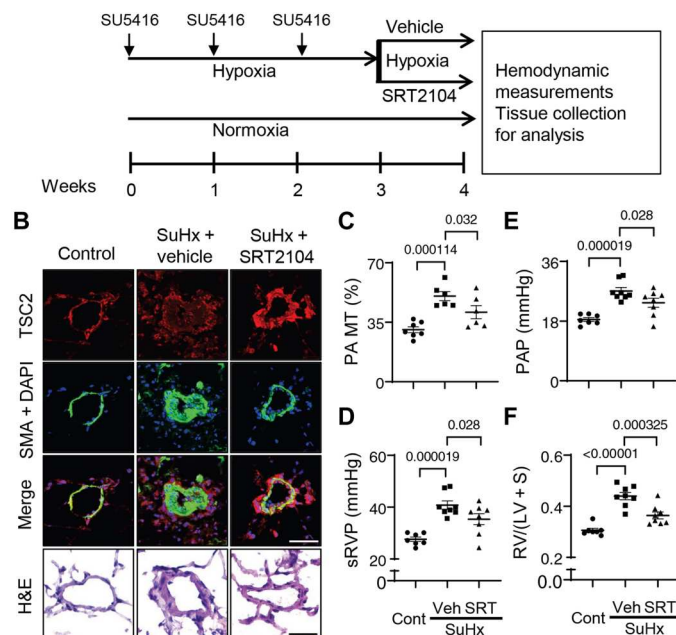
Our proposal of a central role of TSC2 in pulmonary vascular remodeling is further supported by our findings that TSC2 modulated ECM production by PAVSMCs. Reductions in TSC2 abundance in PAVSMCs led to overproduction of two major ECM components, fibronectin and collagen 1 (8, 30), and formation of the abnormal ECM that induces PAH phenotypes. It is also important to note that the decellularized matrix produced by control PAVSMCs with shRNA-induced TSC2 depletion induced the proliferation of not only PAVSMCs but also PAAFs, suggesting that TSC2 also modulates cell-cell communication in the pulmonary vasculature. Our findings agreed with evidence highlighting the importance of cell-matrix and cell-cell communications in PAH pathogenesis (30) and suggest that TSC2 may be an attractive molecular target to disrupt mechanotransduction signaling mediated by YAP and to inhibit ECM remodeling and the associated proliferation of pulmonary vascular cells in PAH.

In TSC2-deficient perivascular epithelioid tumors, YAP accumulation is induced by mTOR through impaired autophagosomal/lysosomal degradation (21). Our findings suggest a mechanism of TSC2-dependent YAP/TAZ and mTOR regulation through the ECM, specifically fibronectin and  $\alpha_5\beta_1$  integrin, and link TSC2 to the PAVSMC proliferative response. Supporting our in vitro findings, SM TSC2 deficiency in mice resulted in stiffening of small PAs, introducing a stiffness-dependent mechanism by which TSC2 regulates YAP in vivo. Stiffening of small PAs occurs as an early event preceding development of pulmonary vascular remodeling and PAH and worsens as the disease progresses (15). Although further studies are needed, it is possible that TSC2 deficiency increases PA wall stiffness through at least two mechanisms, excessive ECM production and activation of mTORC1-dependent PAVSMC proliferation and the resultant wall thickening due to VSMC remodeling. Further, our observations that YAP



**Fig. 5. SRT2104 restores functional TSC2, inhibits proliferation, and induces apoptosis in human PAH PAVSMCs.** (A to G) Human PAH PAVSMCs were treated with diluent (0) or the indicated concentrations of SRT2104 and immunoblotted for the indicated proteins. Data are means  $\pm$  SE from three experiments, each performed on the cells from a different individual. *P* values for SRT2104 treatment compared to diluent (0) were determined by Kruskal-Wallis rank test with Dunn's pairwise comparison. (H) Immunocytochemical analysis to detect fibronectin produced by human nondiseased (control) and PAH PAVSMCs treated with diluent or 10  $\mu\text{M}$  SRT2104 for 48 hours. Scale bar, 100  $\mu\text{m}$ . (I to K) Human PAH PAVSMCs were treated with diluent (–) or 10  $\mu\text{M}$  SRT2104 (+) for 48 hours. Proliferation assessed by cell counts (I) or BrdU incorporation (J) and apoptosis as determined by TUNEL staining (K) analyses were performed. Data are means  $\pm$  SE from three experiments, each performed on the cells from a different individual. *P* values for SRT2104 treatment compared to diluent (0) were determined by Mann-Whitney *U* test. (L) Equal numbers of human control PAVSMCs were seeded on hydrogels with 25-kPa stiffness, treated with diluent (–) or 10  $\mu\text{M}$  SRT2104 (+) for 48 hours, and counted. Data are means  $\pm$  SE from three experiments, each performed on the cells from a different individual. *P* values for SRT2104 treatment compared to diluent (0) were determined by Mann-Whitney *U* test. (M to Q) Immunoblot (M and N), proliferation (as measured by cell counting or BrdU incorporation) (O and P), and apoptosis (as measured by TUNEL staining) (Q) analyses were performed on PAH PAVSMCs transfected with siContr or siTSC2 and treated with 10  $\mu\text{M}$  SRT2104 or diluent for 48 hours. Data are means  $\pm$  SE from three experiments, each performed on the cells from a different individual. *P* values for SRT2104 and/or siTSC2 compared to siContr (Scr) and diluent were determined by Kruskal-Wallis rank test with Dunn's pairwise comparison.

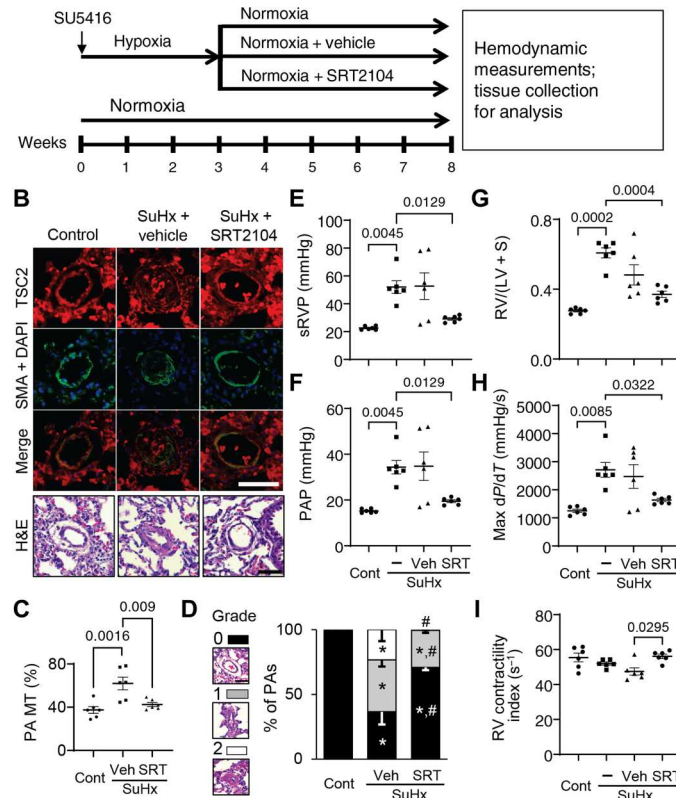


**A** C57/BL6 mice

**Fig. 6. SRT2104 restores TSC2 in small PAs, attenuates PH, and reduces RV hypertrophy in mice.** (A) Six- to 8-week-old male and female mice were maintained under hypoxia for 3 weeks and received SU5416 injection at the beginning of every week. Starting at week 4, mice kept under hypoxia were randomly assigned to receive SRT2104 (SRT) or vehicle (Veh) for 5 days/week for 1 week, and hemodynamic and morphological analyses were performed. Controls were same-age and same-sex mice kept under normoxia. (B) Immunohistochemical analysis to detect TSC2 (red), SMA (green), and DAPI (blue). Images are representative of three mice per group, 12 PAs per mouse. Scale bar, 80  $\mu$ m. For H&E staining, images are representative from seven control mice and six SuHx + vehicle or SuHx + SRT2104, 12 PAs per mouse. Scale bar, 30  $\mu$ m. (C) PA MT was calculated from 12 to 24 PAs per mouse. Data are means  $\pm$  SE from  $n = 7$  control mice (three male, four female),  $n = 6$  PH mice (three male, three female),  $n = 6$  PH + SRT2104 mice (three male, three female) groups.  $P$  values were determined by one-way ANOVA with a Fisher's LSD post hoc test. (D to F) Systolic right ventricular pressure (sRVP) (D), PA pressure (PAP) (E), and Fulton index [RV/(LV + septum) weight ratio] (F) were calculated. Data are means  $\pm$  SE from  $n = 7$  control mice (three male, four female),  $n = 8$  PH mice (four male, four female),  $n = 8$  PH + SRT2104 mice (four male, four female) groups.  $P$  values were determined by one-way ANOVA with a Fisher's LSD post hoc test.

inhibited TSC2 in an ECM-independent manner provide evidence for negative intracellular TSC2-YAP cross-talk that supports unstimulated self-sustained proliferation and resistance to apoptosis of PAVSMCs in PAH.

Our study identified the SIRT1 activator SRT2104 as a potential approach to restore TSC2 abundance and reverse pulmonary vascular remodeling and PH. Reconstitution of TSC2 normalized PAH-specific molecular abnormalities and ECM production, reduced abnormal proliferation, and induced apoptosis in human PAH PAVSMCs. Similar effects were observed in human PAH PAVSMC treated with SRT2104. SIRT1 reduces vascular aging and atherosclerosis in systemic vasculature (45), and its activation improves systemic arterial vascular stiffness in smokers and individuals with type 2 diabetes. SIRT1 stabilizes TSC2 through lysine deacetylation that prevents its degradation (32). We showed that by

**A** Sprague-Dawley rats

**Fig. 7. SRT2104 restores TSC2 in small PAs, attenuates PH, and reduces RV hypertrophy in rats.** (A) Male 6- to 8-week-old rats received one SU5416 injection and were maintained under hypoxia for 3 weeks. Starting in week 4, rats were transferred to normoxia and were randomly assigned to receive SRT2104 (SRT) or vehicle (Veh) for 5 days/week for 5 weeks (days 21 to 56 of the experiment). Upon experiment termination, rats were subjected to hemodynamic and morphological analyses. Controls were same-age untreated male rats kept under normoxia for 8 weeks or exposed to SU5416-hypoxia-normoxia without treatment. (B) Immunohistochemistry was performed for TSC2 (red), SMA (green), and DAPI (blue) and H&E analyses. Scale bar, 50  $\mu$ m. Images are representative from six rats per group, 12 PAs per rat. (C to I) Percentage of fully (grade 2), partially (grade 1), and not occluded PAs (grade 0) was determined (C). Scale bar, 50  $\mu$ m. PA MT (D), sRVP (E), PAP (F), Fulton index (G), RV contractility [max(dP/dT)] (H), and RV contractility index (I) were measured on day 56. Data are means  $\pm$  SE from six rats per group. \* $P < 0.05$  compared to control, # $P < 0.05$  compared to PH.  $P$  values were determined by one-way ANOVA with a Tukey's post hoc test (C), one-way ANOVA with a Fisher's LSD post hoc test (D), and Welch's one-way ANOVA  $F$  test with Games-Howell post hoc analysis (E to I).

restoring TSC2 abundance, SRT2104 reversed the PAH PAVSMC phenotype, reducing proliferation and inducing apoptosis. Orally administered SRT2104 restored smooth muscle TSC2 in small PAs in two animal models of SuHx-induced experimental PH, and even a short treatment of mice with established experimental PH led to reduced pulmonary vascular remodeling, sRVP, and RV hypertrophy, the central clinical features of this disease. Moreover, longer treatment of rats with established experimental PH reversed pulmonary vascular remodeling, sRVP, max dP/dT, and RV hypertrophy and improved the RV contractility index, making SRT2104 a promising drug for therapeutic intervention.

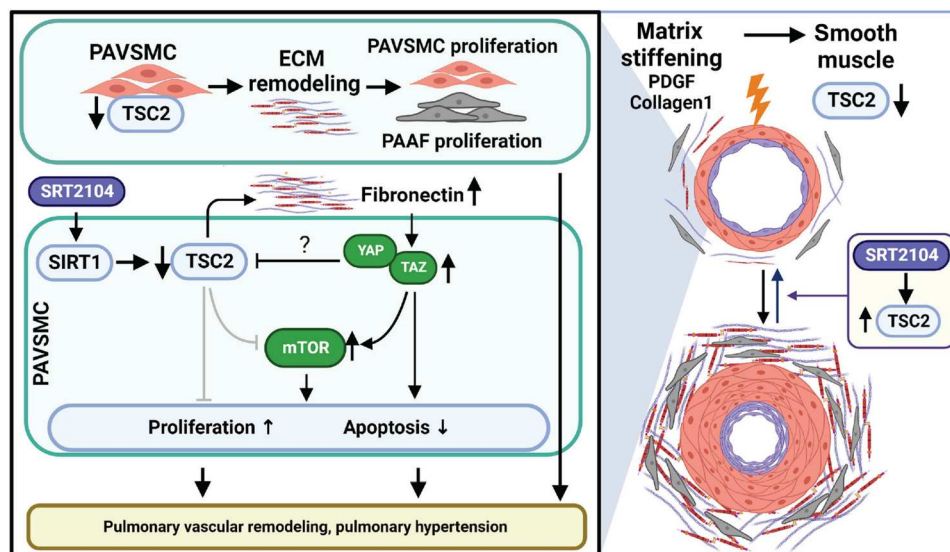


**Fig. 8. Schematic representation of the mechanism by which decreased TSC2 abundance in PAVSMCs promotes pulmonary vascular remodeling and PH.** Decreased TSC2 abundance in PAH PAVSMCs, caused predominantly by the ECM stiffening, results in excessive production of fibronectin, ECM remodeling, overaccumulation of YAP/TAZ, and activation of mTOR, leading to increased proliferation of PAVSMCs and PAAFs, reduced apoptosis of PAVSMCs, pulmonary vascular remodeling, and PH. The SIRT1 activator SRT2104 restores functional TSC2, resolves the molecular and cellular abnormalities caused by decreased TSC2 protein content, and attenuates pulmonary vascular remodeling and PH.

In agreement with our findings, a polyphenol resveratrol that acts at least partially by activating SIRT1 prevents monocrotaline-induced PH in rats (46). However, resveratrol is extensively metabolized in humans, resulting in low systemic bioavailability and limited potential for clinical utility (47). The rapamycin-based mTORC1 inhibitor ABI009 is now in a clinical trial for patients with severe PAH (ClinicalTrials.gov identifier: NCT02587325) and shows promising interim results (48); however, intravenous delivery and reported side effects could make use of this drug challenging for patients with PAH. SRT2104 has better bioavailability than ABI009, demonstrates benefits in preclinical models of age-related disorders (49), is well tolerated in humans, has a favorable selectivity profile (50), and has already entered clinical trials for type 2 diabetes and psoriasis (51, 52), which makes it an attractive candidate for clinical trials for patients with PAH.

We recognize that our study has several limitations. The first limitation is the small human sample size that arises from the nature of the studied disease. PAH is a rare disease, which limits the availability of human lung tissue specimens and early passage cells for mechanistic research of this type. However, the causal role of reduced TSC2 content in mediating PAVSMC hyperproliferation and pulmonary vascular remodeling in PAH was supported by siRNA-mediated depletion in human PAH PAVSMCs and studies of transgenic mice with SMC-specific *Tsc2* deficiency. A second limitation was that not all our *in vitro* experiments used hydrogel matrices to model physiological or pathological stiffness. To separate stiffness-dependent TSC2 functions from their role in ECM remodeling and self-sustained proliferation and survival of PAH PAVSMCs, we collected several datasets from cells cultured on plastic. Although these data agreed with our human tissue-based and hydrogel-derived data, the different substrate may have affected the magnitude of the observed molecular changes. A third limitation was that only male rats were evaluated in the rat

SuHx model of PH, because we did not observe differences between SRT2104-treated male and female SuHx mice. Last, rodent models of PH cannot completely recapitulate human PAH. Moreover, SRT2104 was given to animals as a monotreatment, and the combination of SRT2104 with currently used U.S. Food and Drug Administration–approved therapies was not evaluated. However, given our current findings in cells from PAH individuals and transgenic mice, further testing of targeting TSC2 to reverse PAH is worthy of further investigation.

Despite major progress in PAH treatment within the past decade, there are still no options to reverse advanced disease due to the multifactorial nature of this disease and to the molecular and metabolic reprogramming of pulmonary vascular cells supported by cell-cell and cell-matrix interactions. Our finding that TSC2 links mechanobiological cues, growth factors, and ECM signals with hyperproliferation of PAVSMCs and PAAFs offers a new target for therapeutic intervention. Our preclinical evidence shows that SRT2104, which is already in clinical trials for other diseases and has a favorable safety profile (53), has beneficial effects in human PAH PAVSMCs and two rodent models of PH, warranting further assessment in other preclinical models of PH and perhaps in clinical trials.

## MATERIALS AND METHODS

### Human tissues and cell culture

Human lung tissues from unused donor (control) and idiopathic patients with PAH were provided by the University of Pittsburgh Medical Center Lung Transplant, Pulmonary Division Tissue Donation under protocols approved by the University of Pittsburgh institutional review board. Human primary distal PAVSMCs, primary pulmonary adventitial fibroblasts (PAAFs), and primary PAECs were provided by the Pulmonary Hypertension Breakthrough

Initiative (PHBI) or by the University of Pittsburgh Vascular Medicine Institute (VMI) Cell Processing Core. Cell isolation, characterization, and maintenance were performed under the rigorous and well-established study protocols adopted by the PHBI (7, 8). Briefly, pre-capillary PAs were dissected from the left lower lobe and adherent lung parenchymal tissue using microscissors and scalpel. The arteries were minced to 1-mm<sup>2</sup> blocks and placed on the tissue culture plates with a small drop of LONZA culture medium (LONZA) supplemented with the SmGM-2 or FGM-2 media kit for PAVSMC and PAAF isolation, respectively (7, 8). On the following day, a full volume of respective full growth culture medium was added to the plates, which were left undisturbed for 3 to 5 days. The medium was then subsequently changed every other day until the cells reached confluence. PAVSMCs were characterized using antibodies against three smooth muscle-specific markers (SMA, smooth muscle myosin heavy chain, and SM22; Cell Signaling Technology) and cell morphology (7, 8). PAAFs were characterized using antibodies against vimentin and CD90, and negative staining for SM22, von Willebrand factor (vWF), and cytokeratin (Cell Signaling Technology), to exclude contamination with smooth muscle, endothelial, and epithelial cells, respectively (54). Primary cells (third to eighth passage) of the same passage from a minimum of three control and three PAH individuals were used for each experimental condition. Cells and tissues from deidentified human individuals were used (table S1). Cells were maintained at 37°C in a humidified incubator with 5% CO<sub>2</sub>. For serum deprivation, cells were maintained for 24 to 48 hours in basal PromoCell medium (PromoCell) supplemented with 0.1% bovine serum albumin (BSA) (Thermo Fisher Scientific, Waltham, MA). Softwell hydrogel-coated plates were purchased from Matrigel and used following the manufacturer's protocol. Rat ELT3 cells (CRL-3371; RRID: CVCL\_4616) were purchased from American Type Culture Collection and maintained according to the manufacturer's instructions. The cells were regularly tested for mycoplasma contamination.

### Apoptosis

Apoptosis was measured with the In Situ Cell Death Detection Kit (Roche, Nutley, NJ) based on terminal deoxynucleotidyltransferase-mediated deoxyuridine triphosphate-biotin nick end labeling (TUNEL) technology according to the manufacturer's protocol as previously described (7, 8, 55). Nuclei were detected by 4',6-diamidino-2-phenylindole (DAPI) (Invitrogen). Images were captured by an All-in-One Fluorescence Microscope BZ-X810 (Keyence). Blind semiautomatic counts were performed. A minimum of 200 cells were counted per condition in each experiment.

### Cell proliferation

Cell proliferation was measured by DNA synthesis analysis (BrdU incorporation assay) or Ki67 detection with specific antibody (Cell Signaling Technology) as described previously (7, 8, 55, 56). For the BrdU incorporation assay, cells were serum-deprived for 48 hours, incubated with 10 μM BrdU (Abcam) for 18 hours, fixed with 4% paraformaldehyde in phosphate-buffered saline (PBS; Santa Cruz Biotechnology), permeabilized by 2 M HCl, and stained with anti-BrdU antibody (BD Biosciences). Staining with DAPI and anti-GFP antibody (Cell Signaling Technology) was performed to detect nuclei and GFP, respectively. To detect Ki67, we performed staining with anti-Ki67 antibody and DAPI. Images were taken

using an All-in-One Fluorescence Microscope BZ-X810 (Keyence). Blinded semiautomatic analysis was performed. Cell proliferation was calculated as the percentage of BrdU-positive or Ki67-positive cells per the total number of cells. A minimum of 200 cells were counted in each experiment per each condition. Cell proliferation was performed as described previously (7, 8, 55). Briefly, cells were treated with ATN-161 (MCE LLC), BTT-3033 (R&D Systems), SRT2104 (InvivoChem), or an appropriate diluent. Cells were trypsinized and resuspended in the same volume of basal medium supplemented with 0.1% BSA. Cell counts were performed using the Countess II FL Automated Cell Counter (Thermo Fisher Scientific).

### Immunohistochemical, immunocytochemical, and immunoblot analyses

These analyses were performed as previously described (7, 8, 19, 57). Images were captured with an Olympus FV1000 Confocal Microscope (Olympus America Inc.) or the All-in-One Fluorescence Microscope BZ-X810 (Keyence). Immunoblot signals were captured with HyBlot CL Autoradiography Films (Thomas Scientific), and fixed and developed by Medical Film Processor (Konica Minolta). Densitometry measurements for immunoblots and immunostainings were done with ImageJ [National Institutes of Health (NIH)]. Antibodies for TSC2 (#4308; Research Resource Identifier (RRID): AB\_10547134), cleaved caspase-3 (Asp<sup>175</sup>) (#9661; RRID: AB\_2341188), GFP (#2956; RRID: AB\_1196615), phospho-Ser<sup>235/236</sup>-S6 (#4856; RRID: AB\_2181037), S6 (#2217; RRID: AB\_331355), YAP/TAZ (#8418; RRID: AB\_10950494), phospho-Ser<sup>127</sup>-YAP (#13008; RRID: AB\_2650553), TSC1 (#4906; RRID: AB\_2209790), Rictor (#2114; RRID: AB\_2179963), α/β-tubulin (#2148; RRID: AB\_2288042), phospho-Ser<sup>473</sup>-Akt (#4060; RRID: AB\_2315049), Akt (#9272; RRID: AB\_329827), and anti-rabbit immunoglobulin G (IgG)-horseradish peroxidase (HRP)-linked antibody (#7074; RRID: AB\_2099233) were purchased from Cell Signaling Technology. Anti-fibronectin antibody (ab2413; RRID: AB\_2262874) was purchased from Abcam. Anti-collagen 1A1 antibody (AF6220; RRID: AB\_10891543) was purchased from R&D Systems. Anti-actin and α-smooth muscle-fluorescein isothiocyanate antibody (F3777; RRID: AB\_476977) were purchased from Sigma-Aldrich. Alexa Fluor 488, 594, and 647 dyes, rabbit anti-sheep IgG-HRP-linked antibody (#61-8620; RRID: AB\_2533942), and anti-TSC1 antibody (#PA5-18506; RRID: AB\_10985558) were purchased from Thermo Fisher Scientific.

### Transfection, infection, and decellularization

These procedures were performed as described previously (7, 8, 58). The pEGFP plasmid (#6077-1) was obtained from Addgene. The pEGFP-TSC2 plasmid was previously generated (59, 60). siRNAs and shRNAs were purchased from Dharmacon (PerkinElmer) and Santa Cruz Biotechnology, respectively. siRNA transfection and shRNA infection were performed according to the manufacturers' protocols. Effectene (Qiagen) was used to transfect cells according to the manufacturer's protocol. To produce decellularized matrices, we maintained preconfluent PAVSMCs on plastic plates for 6 days, after which decellularization was performed.



## Animals

All animal procedures were performed under the protocols approved by the Animal Care and Use Committees of the University of Pittsburgh and the University of California, Davis (protocols #17019864 and #21853, respectively). *SM22-Tsc2<sup>+/-</sup>* mice were generated by crossing female *Tsc2<sup>tm1.1Mjg/J</sup>* mice (#027458) with male *SM22-Cre* mice [B6.Cg-Tg(Tagln-cre)1Her/J, #017491] (Jackson Laboratory) carrying mouse *smooth muscle protein 22-alpha* (*SM22*) promoter that induced Cre recombinase expression selectively in VSMCs (61, 62). Mice were genotyped before experiments. The genotyping of the DNA extracted from ears of transgenic mice by the Extract-N-Amp Tissue PCR Kit (Sigma-Aldrich) was performed following the manufacturer's protocol. Polymerase chain reaction (PCR) samples were prepared using the KAPA2G Fast PCR Kit (Sigma-Aldrich) following the manufacturer's protocol. The *SM22-Cre* gene was detected using the primers 5'-GCAATTTTCGGCTATACGTAACAGGG and 5'-GCAAGAACCTGATGGACATGTTTCAG with the internal control primers 5'-CTAGGCCACAGAAATTGAAAGATCT (oIMR7338) and 5'-GTAGGTGGAAATTCTAGCATCC (oIMR7339). *Tsc2* gene was detected with the primers 5'-ACAATGGGAGGCACATTACC and 5'-AAGCAGCAGGTCTGCAGTG. Primers were purchased from Sigma-Aldrich. Control mice were the same age, sex, and background (C57BL/6J, Jackson Laboratories) and housed under the same conditions (8, 63, 64). Experimental PH was induced by SU5416/hypoxia as described previously in (7, 8, 56).

Six- to 8-week-old C57BL/6J mice were randomly assigned to experimental groups and exposed to hypoxia (10% O<sub>2</sub>) for up to 35 days. Subcutaneous injections of SU5416 (20 mg/kg) (Tocris) were performed at days 0, 7, and 14 of the experiment. At days 15 to 21 after experimental PH induction, SRT2104 (InvivoChem) suspended in warm corn oil (ACROS Organics) (100 mg/kg per day, oral gavage, 200  $\mu$ l per mouse) or warm corn oil alone were administered daily. Both male and female mice were used; controls were same-age same-sex mice maintained under normoxia.

Six- to 8-week-old male Sprague-Dawley rats (Charles River Laboratories, Wilmington, MA) received a single dose of SU5416 (sq 20 mg/kg) and were maintained for 3 weeks under hypoxia (10% O<sub>2</sub>) and for 5 weeks under normoxia. Then, animals were randomly assigned to experimental groups. SRT2104 (InvivoChem) in warm corn oil (ACROS Organics) and vehicle (warm corn oil alone) were administered starting at the beginning of week 4 of the experiment for 5 weeks (100 mg per kg per day, oral gavage, 5 days/week). Negative controls were normoxia-maintained age-matched animals. Positive controls were untreated SU5416/hypoxia/normoxia-exposed rats. The volume of the vehicle was equal for the volume of SRT2104 suspension (200  $\mu$ l per mouse or 3 ml per rat). After blinded terminal hemodynamic analysis, animals were euthanized, and lung and heart tissues were collected for morphological analysis. Hearts were separated into RV and LV + septum, and the Fulton index was calculated by the RV/(LV + septum) weight ratio.

Blinded hemodynamic analysis was performed as previously described (8, 56, 64, 65). Briefly, animals were anesthetized by isoflurane (Minrad Inc.): 5% for induction, 2% during surgery, and 1% while performing pressure-volume (PV) loop measurements. PV loop measurements were performed by PV catheters (Scisense Inc.). The catheter attached to the data acquisition system (EMKA Instruments) was inserted into the RV and then into the LV. Data

were acquired by the ADVantage PV System (Transonic Systems Inc.) and IOX2 software (EMKA Technologies Inc.). PAP was calculated as sRVP $\times$ 0.65 + 0.55 mmHg (56, 66). MAP was calculated as sLVP $\times$ 0.65 + 0.55 mmHg (56, 66); RV contractility index was calculated as (max dP/dT)/sRVP s<sup>-1</sup> (56, 67).

Blinded morphological and immunohistological analyses were performed as described previously (7, 8, 19, 55, 56, 65, 68). Briefly, after being perfused by PBS through the PA, lungs were filled with 80% Tissue Plus OCT Compound (Thermo Fisher Scientific)/20% saline solution, snap-frozen in dry ice and kept at -80°C, or fixed in 4% paraformaldehyde solution in PBS and embedded in paraffin. After sectioning, lung tissue slides (5- $\mu$ m thickness) were stained by hematoxylin and eosin (H&E) or immunostained to detect TSC2, SMA, and nuclei (DAPI) (Invitrogen) as previously described (7, 8). Images for PA MT calculation were captured from blind-selected small PAs (25- to 100- $\mu$ m outer diameter from a minimum of six animals per group and a minimum of 12 PAs per animal) of H&E- or SMA-stained rodent lung tissues and calculated using the VMI Calculator (68). The entirety of H&E-stained rat lung tissue sections was captured (six rats per group, minimum of 29 PAs per rat) to count percentage of fully (grade 2), partially (grade 1), and nonoccluded (grade 0) small PAs (25- to 50- $\mu$ m outer diameter) (8, 65, 68–70). Images were taken with an All-in-One Fluorescence Microscope BZ-X810.

## Atomic force microscopy

Lungs were inflated with optimal cutting temperature (OCT) compound (50 ml/kg body weight), frozen in dry ice-cooled 2-methyl butane, and stored at -80°C. Lung parenchymal tissue strips 10  $\mu$ m in thickness were prepared using a cryostat (Leica CM1850), mounted on poly-L-lysine-coated glass slides, stored at -20°C, and measured within 48 hours. Residual OCT was dissolved and rinsed away with PBS immediately before AFM measurements. PAs were identified by morphologic criteria using phase-contrast microscopy. PAs (<200  $\mu$ m in diameter) were mechanically characterized through microindentation using a JPK NanoWizard 4XP Bioscience (Bruker) atomic force microscope. Microindentation was performed using a sphere-tipped probe (Novascan) with a diameter of 5  $\mu$ m and a nominal spring constant of about 60 pN/nm as described (15). The cantilever spring constant was further confirmed at each use by the thermal fluctuation method. This method correlated well with contact-based calibration. The entire AFM system was calibrated by following the manufacturer's instructions before each measurement. Force-indentation profiles were acquired through force scanning at an indentation force of 1 to 2 nN with a Z length of 1.5  $\mu$ m. Force curves were obtained over a 128  $\times$  128 grid of 30 to 80  $\mu$ m in size, depending on the size of the vessel. Young's elastic modulus was calculated by fitting force-indentation data using a Hertz sphere model with JPK data processing software (Bruker). Height and Young's modulus data were converted to 128  $\times$  128 TIFF files and analyzed in ImageJ to allow isolation of only those curves associated with vessel walls. Five to 10 vessels were analyzed per animal.

## Statistical analysis

Statistical comparisons between two groups were performed by the Mann-Whitney *U* test and considered to be statistically different when the *P* value was less than 0.05. Statistical comparisons among three or more groups were performed by the Kruskal-

Wallis test with Dunn's pairwise comparison (all data with sample size  $n < 6$  per group and skewed data with sample size  $n \geq 6$  per group), analysis of variance (ANOVA) test with Fisher's least significant difference (LSD) or Tukey's post hoc test comparison (all data with sample size  $n \geq 6$  per group that satisfied a test of normality assessed using the Kolmogorov-Smirnov test and had equal variances assessed using Bartlett's test), or Welch's one-way ANOVA  $F$  test with Games-Howell post hoc analysis (all data with sample size  $n \geq 6$  per group that satisfied a test of normality but that failed the equal variances assumption test). Statistical analysis was performed using STATA (StataCorp), StatView (SAS Institute), and GraphPad Prism 9.2 (GraphPad Software) software. No animals were excluded from the analysis. To determine animal group sizes, we performed power calculations using G\*Power (release 3.1.9.4) software.

## Supplementary Materials

This PDF file includes:

Figs. S1 to S17

Tables S1 and S2

Other Supplementary Material for this manuscript includes the following:

MDAR Reproducibility Checklist

[View/request a protocol for this paper from Bio-protocol.](#)

## REFERENCES AND NOTES

- M. Humbert, N. W. Morrell, S. L. Archer, K. R. Stenmark, M. R. MacLean, I. M. Lang, B. W. Christman, E. K. Weir, O. Eickelberg, N. F. Voelkel, M. Rabinovitch, Cellular and molecular pathobiology of pulmonary arterial hypertension. *J. Am. Coll. Cardiol.* **43**, S13–S24 (2004).
- A. Hyduk, J. B. Croft, C. Ayala, K. Zheng, Z.-J. Zheng, G. A. Mensah, Pulmonary hypertension surveillance—United States, 1980–2002. *MMWR Surveill. Summ.*, 1–28 (2005).
- M. G. George, L. J. Schieb, C. Ayala, A. Talwalkar, S. Levant, Pulmonary hypertension surveillance: United States, 2001 to 2010. *Chest* **146**, 476–495 (2014).
- A. E. Frost, D. B. Badesch, R. J. Barst, R. L. Benza, C. G. Elliott, H. W. Farber, A. Krichman, T. G. Liou, G. E. Raskob, P. Wason, K. Feldkircher, M. Turner, M. D. McGoon, The changing picture of patients with pulmonary arterial hypertension in the United States. *Chest* **139**, 128–137 (2011).
- C. Guignabert, L. Tu, M. le Hir, N. Ricard, C. Sattler, A. Seferian, A. Huertas, M. Humbert, D. Montani, Pathogenesis of pulmonary arterial hypertension: Lessons from cancer. *Eur. Respir. Rev.* **22**, 543–551 (2013).
- N. W. Morrell, S. Adnot, S. L. Archer, J. Dupuis, P. Lloyd Jones, M. R. MacLean, I. F. McMurtry, K. R. Stenmark, P. A. Thistlethwaite, N. Weissmann, J. X.-J. Yuan, E. K. Weir, Cellular and molecular basis of pulmonary arterial hypertension. *J. Am. Coll. Cardiol.* **54**, S20–S31 (2009).
- D. A. Goncharov, T. V. Kudryashova, H. Ziai, K. Ihida-Stansbury, H. DeLisser, V. P. Krymskaya, R. M. Tuder, S. M. Kawut, E. A. Goncharova, Mammalian target of rapamycin complex 2 (mTORC2) coordinates pulmonary artery smooth muscle cell metabolism, proliferation, and survival in pulmonary arterial hypertension. *Circulation* **129**, 864–874 (2014).
- T. V. Kudryashova, D. A. Goncharov, A. Pena, N. Kelly, R. Vanderpool, J. Baust, A. Kobir, W. Shufesky, A. L. Mora, A. E. Morelli, J. Zhao, K. Ihida-Stansbury, B. Chang, H. DeLisser, R. M. Tuder, S. M. Kawut, H. H. W. Silljé, S. Shapiro, Y. Zhao, E. A. Goncharova, HIPPO–integrin-linked kinase cross-talk controls self-sustaining proliferation and survival in pulmonary hypertension. *Am. J. Respir. Crit. Care Med.* **194**, 866–877 (2016).
- S. S. Pullamsetti, R. Savai, W. Seeger, E. A. Goncharova, Translational advances in the field of pulmonary hypertension. From cancer biology to new pulmonary arterial hypertension therapeutics. Targeting cell growth and proliferation signaling hubs. *Am. J. Respir. Crit. Care Med.* **195**, 425–437 (2017).
- F. A. Masri, W. Xu, S. A. A. Comhair, K. Asosingh, M. Koo, A. Vasanji, J. Drazba, B. Anand-Apte, S. C. Erzurum, Hyperproliferative apoptosis-resistant endothelial cells in idiopathic pulmonary arterial hypertension. *Am. J. Physiol. Lung Cell. Mol. Physiol.* **293**, L548–L554 (2007).
- T. Bertero, K. A. Cottrill, S. Annis, B. Bhat, B. R. Gochuico, J. C. Osorio, I. Rosas, K. J. Haley, K. E. Corey, R. T. Chung, B. Nelson Chau, S. Y. Chan, A YAP/TAZ-miR-130/301 molecular circuit exerts systems-level control of fibrosis in a network of human diseases and physiologic conditions. *Sci. Rep.* **5**, 18277 (2015).
- T. Bertero, W. M. Oldham, K. A. Cottrill, S. Pisano, R. R. Vanderpool, Q. Yu, J. Zhao, Y. Tai, Y. Tang, Y.-Y. Zhang, S. Rehman, M. Sugahara, Z. Qi, J. Gorsan III, S. O. Vargas, R. Saggarr, R. Saggarr, W. D. Wallace, D. J. Ross, K. J. Haley, A. B. Waxman, V. N. Parikh, T. de Marco, P. Y. Hsue, A. Morris, M. A. Simon, K. A. Norris, C. Gaggioli, J. Loscalzo, J. Fessel, S. Y. Chan, Vascular stiffness mechanoactivates YAP/TAZ-dependent glutaminolysis to drive pulmonary hypertension. *J. Clin. Invest.* **126**, 3313–3335 (2016).
- R. Savai, H. M. al-Tamari, D. Sedding, B. Kojonazarov, C. Muecke, R. Teske, M. R. Capocchi, N. Weissmann, F. Grimminger, W. Seeger, R. T. Schermuly, S. S. Pullamsetti, Pro-proliferative and inflammatory signaling converge on FoxO1 transcription factor in pulmonary hypertension. *Nat. Med.* **20**, 1289–1300 (2014).
- T. Bertero, K. A. Cottrill, Y. Lu, C. M. Haeger, P. Dieffenbach, S. Annis, A. Hale, B. Bhat, V. Kaimal, Y.-Y. Zhang, B. B. Graham, R. Kumar, R. Saggarr, R. Saggarr, W. D. Wallace, D. J. Ross, S. M. Black, S. Fratz, J. R. Fineman, S. O. Vargas, K. J. Haley, A. B. Waxman, B. N. Chau, L. E. Fredenburgh, S. Y. Chan, Matrix remodeling promotes pulmonary hypertension through feedback mechanoactivation of the YAP/TAZ-miR-130/301 circuit. *Cell Rep.* **13**, 1016–1032 (2015).
- F. Liu, C. M. Haeger, P. B. Dieffenbach, D. Sicard, I. Chrobak, A. M. F. Coronata, M. M. S. Velandia, S. Vitali, R. A. Colas, P. C. Norris, A. Marinković, X. Liu, J. Ma, C. D. Rose, S.-J. Lee, S. A. A. Comhair, S. C. Erzurum, J. D. McDonald, C. N. Serhan, S. R. Walsh, D. J. Tschumperlin, L. E. Fredenburgh, Distal vessel stiffening is an early and pivotal mechanobiological regulator of vascular remodeling and pulmonary hypertension. *JCI Insight* **1**, e86987 (2016).
- V. P. Krymskaya, E. A. Goncharova, PI3K/mTORC1 activation in hamartoma syndromes: Therapeutic prospects. *Cell Cycle* **8**, 403–413 (2009).
- J. Huang, B. D. Manning, The TSC1–TSC2 complex: A molecular switchboard controlling cell growth. *Biochem. J.* **412**, 179–190 (2008).
- H. Huynh, H.-X. Hao, S. L. Chan, D. Chen, R. Ong, K. C. Soo, P. Pochanard, D. Yang, D. Ruddy, M. Liu, A. Derti, M. N. Balak, M. R. Palmer, Y. Wang, B. H. Lee, D. Sellami, A. X. Zhu, R. Schlegel, A. Huang, Loss of tuberous sclerosis complex 2 (TSC2) is frequent in hepatocellular carcinoma and predicts response to mTORC1 inhibitor everolimus. *Mol. Cancer Ther.* **14**, 1224–1235 (2015).
- V. P. Krymskaya, J. Snow, G. Cesarone, I. Khavin, D. A. Goncharov, P. N. Lim, S. C. Veasey, K. Ihida-Stansbury, P. L. Jones, E. A. Goncharova, mTOR is required for pulmonary arterial vascular smooth muscle cell proliferation under chronic hypoxia. *FASEB J.* **25**, 1922–1933 (2011).
- A. Houssaini, S. Abid, N. Mouraret, F. Wan, D. Rideau, M. Saker, E. Marcos, C.-M. Tissot, J.-L. Dubois-Randé, V. Amselem, S. Adnot, Rapamycin reverses pulmonary artery smooth muscle cell proliferation in pulmonary hypertension. *Am. J. Respir. Cell Mol. Biol.* **48**, 568–577 (2013).
- N. Liang, C. Zhang, P. Dill, G. Panasyuk, D. Pion, V. Koka, M. Gallazzini, E. N. Olson, H. Lam, E. P. Henske, Z. Dong, U. Apte, N. Pallet, R. L. Johnson, F. Terzi, D. J. Kwiatkowski, J.-Y. Scoazec, G. Martignoni, M. Pende, Regulation of YAP by mTOR and autophagy reveals a therapeutic target of tuberous sclerosis complex. *J. Exp. Med.* **211**, 2249–2263 (2014).
- A. Houssaini, S. Abid, G. Derumeaux, F. Wan, A. Parpaleix, D. Rideau, E. Marcos, K. Kebe, G. Czibik, D. Sawaki, C. Treins, J.-L. Dubois-Randé, Z. Li, V. Amselem, L. Lipskaia, M. Pende, S. Adnot, Selective tuberous sclerosis complex 1 gene deletion in smooth muscle activates mammalian target of rapamycin signaling and induces pulmonary hypertension. *Am. J. Respir. Cell Mol. Biol.* **55**, 352–367 (2016).
- V. Cottin, S. Harari, M. Humbert, H. Mal, P. Dorfmueller, X. Jaïs, M. Reynaud-Gaubert, G. Prevot, R. Lazor, C. Taillé, J. Lacronique, S. Zeghar, G. Simonneau, J.-F. Cordier; the Groupe d'Etudes et de Recherche sur les Maladies "Orphelines" Pulmonaires (GERM"O" P), Pulmonary hypertension in lymphangioleiomyomatosis: Characteristics in 20 patients. *Eur. Respir. J.* **40**, 630–640 (2012).
- V. Mieulet, R. F. Lamb, Tuberous sclerosis complex: Linking cancer to metabolism. *Trends Mol. Med.* **16**, 329–335 (2010).
- S. Basu, N. F. Totty, M. S. Irwin, M. Sudol, J. Downward, Akt phosphorylates the Yes-associated protein, YAP, to induce interaction with 14-3-3 and attenuation of p73-mediated apoptosis. *Mol. Cell* **11**, 11–23 (2003).
- Y. Zheng, D. Pan, The hippo signaling pathway in development and disease. *Dev. Cell* **50**, 264–282 (2019).
- N. Kastan, K. Gnedeve, T. Alisch, A. A. Petelski, D. J. Huggins, J. Chiaravalli, A. Aharanov, A. Shakked, E. Tzahor, A. Nagiel, N. Segil, A. J. Hudspeth, Small-molecule inhibition of Lats kinases may promote Yap-dependent proliferation in postmitotic mammalian tissues. *Nat. Commun.* **12**, 3100 (2021).
- H. Tang, J. Chen, D. R. Fraidenburg, S. Song, J. R. Sysol, A. R. Drennan, S. Offermanns, R. D. Ye, M. G. Bonini, R. D. Minshall, J. G. N. Garcia, R. F. Machado, A. Makino, J. X.-J. Yuan, Deficiency

- of Akt1, but not Akt2, attenuates the development of pulmonary hypertension. *Am. J. Physiol. Lung Cell. Mol. Physiol.* **308**, L208–L220 (2014).
29. E. A. Goncharova, D. A. Goncharov, A. Eszterhas, D. S. Hunter, M. K. Glassberg, R. S. Yeung, C. L. Walker, D. Noonan, D. J. Kwiatkowski, M. M. Chou, R. A. Panettieri Jr., V. P. Krymskaya, Tuberin regulates p70 S6 kinase activation and ribosomal protein S6 phosphorylation: A role for the TSC2 tumor suppressor gene in pulmonary lymphangioleiomyomatosis (LAM). *J. Biol. Chem.* **277**, 30958–30967 (2002).
  30. T. Thenappan, S. Y. Chan, E. K. Weir, Role of extracellular matrix in the pathogenesis of pulmonary arterial hypertension. *Am. J. Physiol. Heart Circ. Physiol.* **315**, H1322–H1331 (2018).
  31. H. Chong-Kopera, K. Inoki, Y. Li, T. Zhu, F. R. Garcia-Gonzalo, J. L. Rosa, K.-L. Guan, TSC1 stabilizes TSC2 by inhibiting the interaction between TSC2 and the HERC1 ubiquitin ligase. *J. Biol. Chem.* **281**, 8313–8316 (2006).
  32. A. García-Aguilar, C. Guillén, M. Nellist, A. Bartolomé, M. Benito, TSC2 N-terminal lysine acetylation status affects its stability modulating mTORC1 signaling and autophagy. *Biochim. Biophys. Acta* **1863**, 2658–2667 (2016).
  33. D. Nagata, R. Takeda, M. Sata, H. Satonaka, E. Suzuki, T. Nagano, Y. Hirata, AMP-activated protein kinase inhibits angiotensin II-stimulated vascular smooth muscle cell proliferation. *Circulation* **110**, 444–451 (2004).
  34. L. J. Rubin, L. Magliola, X. Feng, A. W. Jones, C. C. Hale, Metabolic activation of AMP kinase in vascular smooth muscle. *J. Appl. Physiol.* **98**, 296–306 (2005).
  35. D. B. Shackelford, R. J. Shaw, The LKB1-AMPK pathway: Metabolism and growth control in tumour suppression. *Nat. Rev. Cancer* **9**, 563–575 (2009).
  36. A. Szwed, E. Kim, E. Jacinto, Regulation and metabolic functions of mTORC1 and mTORC2. *Physiol. Rev.* **101**, 1371–1426 (2021).
  37. E. A. Goncharova, V. P. Krymskaya, Pulmonary lymphangioleiomyomatosis (LAM): Progress and current challenges. *J. Cell. Biochem.* **103**, 369–382 (2008).
  38. K. R. Stenmark, R. P. Mecham, Cellular and molecular mechanisms of pulmonary vascular remodeling. *Annu. Rev. Physiol.* **59**, 89–144 (1997).
  39. W. Sun, S. Y. Chan, Pulmonary arterial stiffness: An early and pervasive driver of pulmonary arterial hypertension. *Front. Med. (Lausanne)* **5**, 204–204 (2018).
  40. P. B. Dieffenbach, C. M. Haeger, A. M. F. Coronata, K. M. Choi, X. Varelas, D. J. Tschumperlin, L. E. Fredenburgh, Arterial stiffness induces remodeling phenotypes in pulmonary artery smooth muscle cells via YAP/TAZ-mediated repression of cyclooxygenase-2. *Am. J. Physiol. Lung Cell. Mol. Physiol.* **313**, L628–L647 (2017).
  41. N. W. Morrell, S. L. Archer, A. De Felice, S. Evans, M. Fisman, T. Martin, M. Saulnier, M. Rabinovitch, R. Schermuly, D. Stewart, H. Truebel, G. Walker, K. R. Stenmark, Anticipated classes of new medications and molecular targets for pulmonary arterial hypertension. *Pulm. Circ.* **3**, 226–244 (2013).
  42. E. A. Goncharova, D. A. Goncharov, A. Eszterhas, D. S. Hunter, M. K. Glassberg, R. S. Yeung, C. L. Walker, D. Noonan, D. J. Kwiatkowski, M. M. Chou, R. A. Panettieri Jr., V. P. Krymskaya, Tuberin regulates p70 S6 kinase activation and ribosomal protein S6 phosphorylation: A role for the TSC2 tumor suppressor gene in pulmonary lymphangioleiomyomatosis. *J. Biol. Chem.* **277**, 30958–30967 (2002).
  43. A. Weiss, M. C. Neubauer, D. Yerabolu, B. Kojonazarov, B. C. Schlueter, L. Neubert, D. Jonigk, N. Baal, C. Ruppert, P. Dorfmueller, S. S. Pullamsetti, N. Weissmann, H.-A. Ghofrani, F. Grimminger, W. Seeger, R. T. Schermuly, Targeting cyclin-dependent kinases for the treatment of pulmonary arterial hypertension. *Nat. Commun.* **10**, 2204 (2019).
  44. S. A. Barman, S. Zhu, R. E. White, RhoA/Rho-kinase signaling: A therapeutic target in pulmonary hypertension. *Vasc. Health Risk Manag.* **5**, 663–671 (2009).
  45. M. S. Bonkowski, D. A. Sinclair, Slowing ageing by design: The rise of NAD<sup>+</sup> and sirtuin-activating compounds. *Nat. Rev. Mol. Cell Biol.* **17**, 679–690 (2016).
  46. A. Csizsar, N. Labinskyy, S. Olson, J. T. Pinto, S. Gupte, J. M. Wu, F. Hu, P. Ballabh, A. Podlutzky, G. Losonczy, R. de Cabo, R. Mathew, M. S. Wolin, Z. Ungvari, Resveratrol prevents monocrotaline-induced pulmonary hypertension in rats. *Hypertension* **54**, 668–675 (2009).
  47. M. D. Knutson, C. Leeuwenburgh, Resveratrol and novel potent activators of Sirt1: Effects on aging and age-related diseases. *Nutr. Rev.* **66**, 591–596 (2008).
  48. M. Simon, M. Gombert-Maitland, R. Oudiz, R. Machado, F. Rischard, J. Elinoff, B. Grigorian, A. Schmid, S. Hou, N. Desai, M. Gladwin, Patients with severe pulmonary arterial hypertension treated with ABI-009, nab-sirolimus, an mTOR inhibitor: Interim results from a phase 1 clinical trial. *J. Am. Coll. Cardiol.* **73**, 1927–1927 (2019).
  49. X. Zhang, X. Li, J. Zhang, Current status and future perspectives of PI3K and mTOR inhibitor as anticancer drugs in breast cancer. *Curr. Cancer Drug Targets* **13**, 175–187 (2013).
  50. E. Hoffmann, J. Wald, S. Lavu, J. Roberts, C. Beaumont, J. Haddad, P. Elliott, C. Westphal, E. Jacobson, Pharmacokinetics and tolerability of SRT2104, a first-in-class small molecule activator of SIRT1, after single and repeated oral administration in man. *Br. J. Clin. Pharmacol.* **75**, 186–196 (2013).
  51. S. Venkatasubramanian, R. M. Noh, S. Daga, J. P. Langrish, N. L. Mills, B. R. Waterhouse, E. Hoffmann, E. W. Jacobson, N. N. Lang, B. M. Frier, D. E. Newby, Effects of the small molecule SIRT1 activator, SRT2104 on arterial stiffness in otherwise healthy cigarette smokers and subjects with type 2 diabetes mellitus. *Open Heart* **3**, e000402 (2016).
  52. A. Baksi, O. Kraydashenko, A. Zalevkaya, R. Stets, P. Elliott, J. Haddad, E. Hoffmann, G. P. Vlasuk, E. W. Jacobson, A phase II, randomized, placebo-controlled, double-blind, multi-dose study of SRT2104, a SIRT1 activator, in subjects with type 2 diabetes. *Br. J. Clin. Pharmacol.* **78**, 69–77 (2014).
  53. J. G. Krueger, M. Suárez-Fariñas, I. Cueto, A. Khacharian, R. Matheson, L. C. Parish, C. Leonardi, D. Shortino, A. Gupta, J. Haddad, G. P. Vlasuk, E. W. Jacobson, A randomized, placebo-controlled study of SRT2104, a SIRT1 activator, in patients with moderate to severe psoriasis. *PLOS ONE* **10**, e0142081 (2015).
  54. D. Wang, H. Zhang, M. Li, M. G. Frid, A. R. Flockton, B. A. McKeon, M. E. Yeager, M. A. Fini, N. W. Morrell, S. S. Pullamsetti, S. Velegala, W. Seeger, T. A. McKinsey, C. C. Sucharov, K. R. Stenmark, MicroRNA-124 controls the proliferative, migratory, and inflammatory phenotype of pulmonary vascular fibroblasts. *Circ. Res.* **114**, 67–78 (2014).
  55. E. A. Goncharova, D. A. Goncharov, H. Li, W. Pimtong, S. Lu, I. Khavin, V. P. Krymskaya, mTORC2 is required for proliferation and survival of TSC2-null cells. *Mol. Cell. Biol.* **31**, 2484–2498 (2011).
  56. Y. Shen, D. A. Goncharov, T. Avolio, A. Ray, E. Okorie, H. De Lissier, A. L. Mora, R. Vanderpool, T. V. Kudryashova, E. A. Goncharova, Differential effects of integrin-linked kinase inhibitor Cpd22 on severe pulmonary hypertension in male and female rats. *Pulm. Circ.* **10**, 2045894019898593 (2020).
  57. E. A. Goncharova, D. A. Goncharov, V. P. Krymskaya, Assays for in vitro monitoring of human airway smooth muscle (ASM) and human pulmonary arterial vascular smooth muscle (VSM) cell migration. *Nat. Protoc.* **1**, 2933–2939 (2006).
  58. M. Parmaksiz, A. E. Elçin, Y. M. Elçin, Decellularized cell culture ECMs act as cell differentiation inducers. *Stem Cell Rev. Rep.* **16**, 569–584 (2020).
  59. E. Goncharova, D. Goncharov, D. Noonan, V. P. Krymskaya, TSC2 modulates actin cytoskeleton and focal adhesion through TSC1-binding domain and the Rac1 GTPase. *J. Cell Biol.* **167**, 1171–1182 (2004).
  60. G. A. Finlay, B. York, R. H. Karas, B. L. Fanburg, H. Zhang, D. J. Kwiatkowski, D. J. Noonan, Estrogen-induced smooth muscle cell growth is regulated by tuberin and associated with altered activation of platelet-derived growth factor receptor-beta and ERK-1/2. *J. Biol. Chem.* **279**, 23114–23122 (2004).
  61. R. Lesche, M. Groszer, J. Gao, Y. Wang, A. Messing, H. Sun, X. Liu, H. Wu, Cre/loxP-mediated inactivation of the murine Pten tumor suppressor gene. *Genesis* **32**, 148–149 (2002).
  62. F. Schwenk, U. Baron, K. Rajewsky, A cre-transgenic mouse strain for the ubiquitous deletion of loxP-flanked gene segments including deletion in germ cells. *Nucleic Acids Res.* **23**, 5080–5081 (1995).
  63. J. Meloche, A. Pfeleger, M. Vaillancourt, R. Paulin, F. Potus, S. Zervopoulos, C. Graydon, A. Courboulain, S. Breuils-Bonnet, È. Tremblay, C. Couture, E. D. Michelakis, S. Provencher, S. Bonnet, Role for DNA damage signaling in pulmonary arterial hypertension. *Circulation* **129**, 786–797 (2014).
  64. L. Taraseviciene-Stewart, Y. Kasahara, L. Alger, P. Hirth, G. McMahon, J. Waltenberger, N. F. Voelkel, R. M. Tuder, Inhibition of the VEGF receptor 2 combined with chronic hypoxia causes cell death-dependent pulmonary endothelial cell proliferation and severe pulmonary hypertension. *FASEB J.* **15**, 427–438 (2001).
  65. A. Pena, A. Kobir, D. Goncharov, A. Goda, T. V. Kudryashova, A. Ray, R. Vanderpool, J. Baust, B. Chang, A. L. Mora, J. Gorscan III, E. A. Goncharova, Pharmacological inhibition of mTOR kinase reverses right ventricle remodeling and improves right ventricle structure and function in rats. *Am. J. Respir. Cell Mol. Biol.* **57**, 615–625 (2017).
  66. R. Syeed, J. T. Reeves, D. Welsh, D. Raeside, M. K. Johnson, A. J. Peacock, The relationship between the components of pulmonary artery pressure remains constant under all conditions in both health and disease. *Chest* **133**, 633–639 (2008).
  67. D. T. Mason, E. Braunwald, J. W. Covell, E. H. Sonnenblick, J. Ross Jr., Assessment of cardiac contractility. The relation between the rate of pressure rise and ventricular pressure during isovolumic systole. *Circulation* **44**, 47–58 (1971).
  68. E. E. Kelley, J. Baust, G. Bonacci, F. Golin-Bisello, J. E. Devlin, C. M. St. Croix, S. C. Watkins, S. Gor, N. Cantu-Medellin, E. R. Weidert, J. C. Frisbee, M. T. Gladwin, H. C. Champion, B. A. Freeman, N. K. H. Khoo, Fatty acid nitroalkenes ameliorate glucose intolerance and pulmonary hypertension in high-fat diet-induced obesity. *Cardiovasc. Res.* **101**, 352–363 (2014).
  69. M. Oka, N. Homma, L. Taraseviciene-Stewart, K. G. Morris, D. Kraskauskas, N. Burns, N. F. Voelkel, I. F. McMurtry, Rho kinase-mediated vasoconstriction is important in severe occlusive pulmonary arterial hypertension in rats. *Circ. Res.* **100**, 923–929 (2007).
  70. S. Gairhe, S. R. Joshi, M. M. Bastola, J. M. McLendon, M. Oka, K. A. Fagan, I. F. McMurtry, Sphingosine-1-phosphate is involved in the occlusive arteriopathy of pulmonary arterial hypertension. *Pulm. Circ.* **6**, 369–380 (2016).



**Acknowledgments:** We thank A. Sebastiani and the Small Animal Hemodynamic Core at the University of Pittsburgh Heart, Lung, and Blood Vascular Medicine Institute (VMI) for the acquisition and analysis of animal hemodynamic data. We thank the Pulmonary Hypertension Breakthrough Initiative (PHBI) and the University of Pittsburgh VMI Cell Processing Core for providing lung tissues and pulmonary vascular cells from patients with PAH and unused donor lungs. We thank J. Sembrat from the University of Pittsburgh School of Medicine for help with the acquisition of human tissues. **Funding:** This work is supported by NIH/NHLBI R01HL113178 (E.A.G.), R01HL130261 (E.A.G.), R01HL150638 (E.A.G.), 5P01HL103455-05 (A.L.M. and E.A.G.), 1U01HL145550 (M.R.), 5P50AR060780 (M.R.), and American Heart Association Postdoctoral Fellowship 826806 (Y.S.). The PHBI is supported by NIH/NHLBI R24HL123767. L.E.F.'s work related to PH is supported by NIH/NHLBI and American Heart Association. **Author contributions:** Y.S., D.A.G., A.P., J.B., A.C.B., A. Ray, A. Rode, B.C., M.R., P.D., L.E.F., L.J., T.V.K., and E.A.G. acquired the data. Y.S., D.A.G., A.P., B.C., T.N.B., H.D., A.L.M., M.R., P.D., L.E.F., L.J., T.V.K., and

E.A.G. analyzed and interpreted the data. Y.S. and E.A.G. conceived and designed the research. H.D. contributed human pulmonary vascular cells. Y.S., H.D., A.L.M., P.D., L.E.F., and E.A.G. drafted and edited the manuscript. **Competing interests:** The authors declare that they have no competing interests. **Data and materials availability:** All data needed to evaluate the conclusions in the paper are present in the paper or the Supplementary Materials. The *SM22-Tsc<sup>+/−</sup>* mice are available from E.A.G. under a material transfer agreement from the Jackson Laboratories and from the University of California, Davis.

Submitted 15 November 2021

Accepted 15 November 2022

Published 6 December 2022

10.1126/scisignal.abn2743

## Cross-talk between TSC2 and the extracellular matrix controls pulmonary vascular proliferation and pulmonary hypertension

Yuanjun Shen, Dmitry A. Goncharov, Andressa Pena, Jeffrey Baust, Andres Chavez Barragan, Arnab Ray, Analise Rode, Timothy N. Bachman, Baojun Chang, Lifeng Jiang, Paul Dieffenbach, Laura E. Fredenburgh, Mauricio Rojas, Horace DeLisser, Ana L. Mora, Tatiana V. Kudryashova, and Elena A. Goncharova

*Sci. Signal.*, **15** (763), eabn2743.

DOI: 10.1126/scisignal.abn2743

### Protection from pulmonary hypertension

Pulmonary arterial hypertension (PAH) is partially driven by the proliferation of pulmonary arterial vascular smooth muscle cells (PAVSMCs) induced by stiffening of pulmonary arteries. The GTPase-activating protein TSC2 inhibits cell growth-promoting signaling, leading Shen et al. to characterize how TSC2 might prevent the pathogenesis of PAH. Pulmonary arteries and PAVSMCs from PAH patients had reduced TSC2 abundance, and pulmonary artery remodeling and hypertension developed in mice with partial deficiency of TSC2 in smooth muscle. Analysis of PAVSMCs suggested that the stiffening of pulmonary arteries in PAH led to a decrease in TSC2 content in smooth muscle, triggering remodeling of the extracellular matrix, activation of mechanosensitive and cell growth signaling pathways, and increased PAVSMC proliferation. Restoring TSC2 abundance in rodent models with a drug currently in clinical trials improved lung function and reduced pulmonary hypertension. Thus, strategies that increase TSC2 abundance in PAVSMCs may reverse PAH, a condition that is ultimately fatal and that currently lacks effective treatments. –WW

### View the article online

<https://www.science.org/doi/10.1126/scisignal.abn2743>

### Permissions

<https://www.science.org/help/reprints-and-permissions>

Use of this article is subject to the [Terms of service](#)

*Science Signaling* (ISSN ) is published by the American Association for the Advancement of Science. 1200 New York Avenue NW, Washington, DC 20005. The title *Science Signaling* is a registered trademark of AAAS.

Copyright © 2022 The Authors, some rights reserved; exclusive licensee American Association for the Advancement of Science. No claim to original U.S. Government Works